Universidade Federal de Viçosa - UFV

Centro de Ciências Exatas e Tecnológicas - CCE

Departamento de Engenharia Elétrica - DEL

ELECTROCOAGULATION SYSTEM SUPPLIED BY PHOTOVOLTAIC PANELS IN STAND ALONE APPLICATIONS: THE BUCK CONVERTERS CONTROL DESIGN

William Caires Silva Amorim

Orientador : Prof. Dr. Heverton Augusto Pereira

Viçosa, 03 de Maio de 2018.

Universidade Federal de Viçosa - UFV

Centro de Ciências Exatas e Tecnológicas - CCE

Departamento de Engenharia Elétrica - DEL

ELECTROCOAGULATION SYSTEM SUPPLIED BY PHOTOVOLTAIC PANELS IN STAND ALONE APPLICATIONS: THE BUCK CONVERTERS CONTROL DESIGN

William Caires Silva Amorim

Trabalho de Conclusão de Curso submetido ao Departamento de Engenharia Elétrica da Universidade Federal de Viçosa para a obtenção dos créditos referentes à disciplina Monografia e Seminário do curso de Engenharia Elétrica.

Orientador : Prof. Dr. Heverton Augusto Pereira
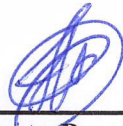
Viçosa, 03 de Maio de 2018.

WILLIAM CAIRES SILVA AMORIM

ELECTROCOAGULATION SYSTEM SUPPLIED BY PHOTOVOLTAIC PANELS IN STAND ALONE APPLICATIONS: THE BUCK CONVERTERS CONTROL DESIGN
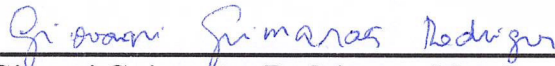
Monografia apresentada ao Departamento de Engenharia Elétrica do Centro de Ciências Exatas e Tecnológicas da Universidade Federal de Viçosa, para a obtenção dos créditos da disciplina ELT 490 – Monografia e Seminário e cumprimento do requisito parcial para obtenção do grau de Bacharel em Engenharia Elétrica.
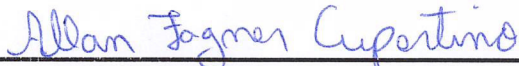
Aprovada em 03 de Maio de 2018.

COMISSÃO EXAMINADORA

Prof. Dr. Heverton Augusto Pereira - Orientador
Universidade Federal de Viçosa - UFV

Prof. Dr. Giovani Guimarães Rodrigues - Membro
Centro Federal de Educação Tecnológica de Minas Gerais - CEFET-MG

Prof. M. Sc. Allan Fagner Cupertino - Membro
Centro Federal de Educação Tecnológica de Minas Gerais - CEFET-MG

Eng. Lucas Santana Xavier - Membro
Mestrando na Universidade Federal de Minas Gerais - UFMG

À minha família,
mentores e amigos.

"I have the impression that I was a child playing at the seashore, amusing myself to discover a flatter pebble or a shell more beautiful than the others, while the immense ocean of truth remains mysterious before my eyes."

Isaac Newton

Agradecimentos

Agradeço a Deus por ter me iluminado em todos os passos nesta jornada acadêmica, e sobretudo aos meus pais Maria e Almir, por serem meu porto seguro e terem apoiado meus passos por todos estes anos. Aos professores da graduação, em especial ao Prof. Heverton Pereira que me orientou durante este trabalho e outros estudos no GESEP. E aos amigos da graduação e do GESEP por toda a ajuda oferecida no decorrer destes semestres, em especial à Dayane, Paulo, Weverton, João Marcus, Lucas Gusman e Rafael, auxiliando em diversas dúvidas e questionamentos e sendo fundamentais para trilhar esta jornada da graduação.

Sumário

Resumo

Os sistemas elétricos autônomos são caracterizados por sua operação independente de uma rede de distribuição de energia elétrica, situação presente em algumas áreas rurais e locais remotos. Neste caso o sistema fotovoltaico é uma das fontes mais conhecidas e aplicada para fornecerem energia elétrica. Em momentos em que a geração de energia for maior que o consumo, o excedente pode ser enviado a um banco de baterias (BB), utilizado quase que inerente ao sistema, para que possa alimentar a carga. Devido às dificuldades políticas e estruturais, no Brasil em especial, as conhecidas estações de tratamento de água (ETAs) não estão disponíveis para atender toda a população. Em termos de potabilização de água, o processo de clarificação é uma das etapas fundamentais, e o reator de eletrocoagulação vem se destacando em diversos estudos quanto ao método convencional de adição de Sulfato de Alumínio $Al_2(SO_4)_3$. Neste contexto, um sistema autônomo de eletrocoagulação (AES) é proposto no desenvolvimento deste trabalho. Maior destaque é obtido com a integração efetuada entre o painel fotovoltaico, banco de baterias e eletrocoagulador. Como perturbação externa a este sistema temos a variação da irradiação solar, que insere uma dinâmica durante um certo período e requer soluções de máxima extração de energia dos painéis fotovoltaicos. O tradicional método de rastreamento de máxima potência (MPPT), conhecido como algoritmo perturba e observa (P&O), revela-se um importante meio para obter tal resultado, na conexão efetuada entre o painel fotovoltaico e o banco de baterias. Toda a integração entre os três elementos principais deste sistema é feita com conversores c.c. da topologia buck, responsáveis por reduzir a tensão do painel fotovoltaico. Os ganhos dos conversores buck são calculados a partir do método de alocação de polos. As análises propostas neste trabalho são relativas á eficácia do método MPPT implementado e ao controle projetado. Assim, a capacidade dos controladores implementados é analisada, conferindo a sua dinâmica e capacidade de seguir as referências impostas, utilizando para isto os ganhos projetados. As demais características, como eficiência dinâmica e estática do MPPT implementado, perdas de chaveamento e condução nos semicondutores, entre outros são abordadas neste trabalho. Os resultados comprovam a eficácia e validade da integração necessária para funcionamento do sistema autônomo de eletrocoagulação proposto, além de ótimos índices de eficiência do sistema integrado e do algoritmo MPPT implementado.

Abstract

The autonomous electrical systems are characterized by their operation independent of a distribution network of electric power, a condition present in some rural areas and remote locations. In such conditions the photovoltaic system is one of the most well-known sources and applied to provide electricity. When power generation is greater than consumption, surplus can be sent to a battery bank (BB), used almost inherently in the system, to feed the load. Due to the political and structural difficulties, in Brazil in particular, the known water treatment plants (WTPs) are not available to serve the entire population. In terms of water purification, the clarification process is one of the fundamental steps, and the electrocoagulation reactor has been highlighted in several studies regarding the conventional method based on addition of Aluminum Sulphate $Al_2(SO_4)_3$. In this context, an autonomous electrocoagulation system (AES) is proposed in the development of this work. Higher emphasis is achieved with the integration between the photovoltaic panel, battery bank and electrocoagulator. Variation of the solar irradiation is an external disturbance to this system, which inserts a dynamics during a certain period and requires solutions of maximum energy extraction of the photovoltaic panels. The traditional maximum power tracking (MPPT) method, known as the perturbation and observation algorithm (P&O), proves to be an important means to obtain such a result in the connection between the PV panel and the battery bank. All integration between the three main elements of this system is done with c.c. of the topology buck, responsible for reducing the voltage of the photovoltaic panel. The control gains are modeled from the pole allocation method. The analyzes proposed in this work are related to the effectiveness of the implemented MPPT method and the designed control. Thus, the capacity of the implemented controllers is analyzed, giving their dynamics and ability to follow the imposed references, using the projected gains. The other characteristics, such as the dynamic and static efficiency of MPPT implemented, loss of switching and conduction in the semiconductors, among others are discussed in this work. The results confirm the effectiveness and validity of the integration required for the operation of the proposed autonomous electrocoagulation system, as well as the excellent efficiency indexes of the integrated system and MPPT algorithm implemented.

Lista de Tabelas

Lista de Figuras

List of Symbols

small letter   quantities varying in time;
CAPITAL LETTER   quantities and parameters constant;

V_{mp}	Maximum Power Voltage
V_{bat}	Battery Voltage
d	duty cycle
C_{crit}	Critical Capacitance
L_{crit}	Critical Inductance
v_{eq}	Equivalent Voltage of the PVP
R_{eq}	Equivalent Resistance of the PVP
C_{pv}	Capacitance in Parallel with the PVP
v_{pv}	PVP Output Voltage
i_{pv}	PVP Output Current
d_1	Duty Cycle in buck Converter 1
i_{L1}	Current in Inductor of the buck Converter 1
R_{L1}	Resistance of the buck Converter 1
L_1	Inductance of the buck Converter 1
v_{bat}	BB Output Voltage
i_{bat}	BB Output Current
d_2	Duty Cycle in buck Converter 2
i_{L2}	Current in Inductor of the buck Converter 2
R_{L2}	Resistance of the buck Converter 2
L_2	Inductance of the buck Converter 2
C	Capacitance in Parallel with the EC
i_{load}	Current in the EC
R_{load}	Resistance in the EC
v_{load}	Voltage in the EC

m	Aluminum Concentration in the Water
T_j	Temperature of the Junction
T_c	Temperature of the Case
T_h	Temperature of the Heat Sink
T_a	Temperature of the Ambient
R_{jc}	Resistance between Junction and Case
R_{ch}	Resistance between Case and Heat Sink
R_{ha}	Resistance between Heat Sink and Ambient
R_{ja}	Resistance between junction and Ambient
N_S	Series Cells of the PVP
N_P	Parallel Cells of the PVP
N_s	Series Cells of the BB
N_p	Parallel Cells of the BB
C_{term}	Capacitance Cell of the BB
K_{P1}	Proportional Gain of the Internal Mesh (buck Converter 1)
K_{I1}	Integral Gain of the Internal Mesh (buck Converter 1)
K_{P2}	Proportional Gain of the Internal Mesh (buck Converter 1)
K_{I2}	Integral Gain of the Internal Mesh (buck Converter 1)
K_{P3}	Proportional Gain of the buck Converter 2
K_{I3}	Integral Gain of the buck Converter 2
f_{sw}	Switching frequency
f_s	Sample frequency
I_{rad}	Solar Irradiation incident on the PVP
p_{MA}	Open mesh Pole

Superscripts

$*$	Reference value

List of Abbreviations

AES   Autonomous Electrocoagulation Systems

WTS   Water Treatment Station

BB   Battery Bank

EC   Electrocoagulator

PS   Photovoltaic System

PVP   Photovoltaic Panel

SOC   State of Charge

P&O   perturb and observes

MPPT   Maximum Power Point Tracking

EEC   Equivalent Electrical Circuit

EDA   Electronic Design Automation

PWM   Pulse Width Modulation

Introduction

The raw water used for purification in Brazil are collected from surface and underground water bodies, which must comply with specific characteristics (Pinto et al, 2012). Depending on the degree of concentration of pollutants and components which are undesirable for human consumption, they should be removed by different treatment steps. In station for water treatments (WTS) in Brazil, the full-cycle treatment generally consists of six main steps: capture, coagulation, flocculation, decantation, filtration and disinfection of water. The clarification process, presented in Fig. (1.1), summarizes the steps of coagulation and flocculation, which are responsible to transform the substances in the form of fine suspension and colloidal suspension into larger particles (flakes), thus, they can be removed by decanting and filtration (Dubrawski and Mohseni, 2013; Harif et al, 2012). Despite the availability of surface water effluent treatments, alternatives treatments such as electrocoagulation have been studied (Combatt et al, 2017).

Among the several technologies, electrocoagulation stands out with the use of aluminum electrodes. This equipment has several advantages over the conventional method of chemical addition for coagulation and flocculation. Besides, it is easy to operate and maintain, as well as to avoid chemical contamination (by quantities high chemical neutralizers), rapid filtering of the residues and the process can be controlled electrically (Mollaha et al, 2004).

The portability imposed by the use of an electrocoagulator (EC) allows the expansion of the clarification process to remote areas and with the possibility of using solar energy as a source to feed the system. Thus, it is possible
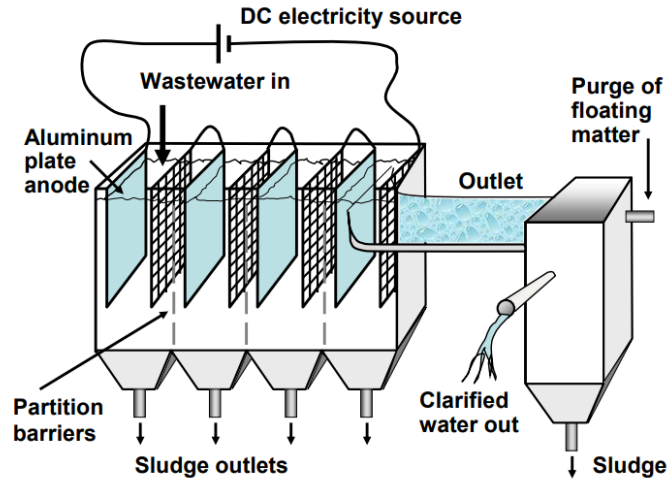
Figura 1.1: Electrocoagulation system in a process of Clarification (Hernández-Calderón et al, 2011).

to extend this project to remote communities, where it would be difficult to install a conventional WTS. Photovoltaic systems have gained prominence among the renewable energy sources due to its low environmental impact, quiet operation and easy aggregation to the structures. Thus, some authors have recommended its use for small applications, and emphasized its efficiency in locations far away from the urban center (Alvarez-Guerra et al, 2011; Zhang et al, 2013; Valero et al, 2008; Ortiz et al, 2007; Marmanis et al, 2015).

Depending on the distance of the place, it is not feasible to carry long transmission lines to remote places with low population. In this way this project becomes attractive. The EC use can be justified because government programs have prioritized the installation of stand alone photovoltaic systems destined mainly to the illumination, cooling and water pumping (Marmanis et al, 2015). These stand alone systems are a vector of social and economic development, facilitating access to health services, education, water supply and sanitation. Thus, the right of people living in rural areas to access improved water sources should be seen as a global challenge. Besides, the solution of the water treatment problem, depends on the creation and implementation of sustainable management strategies for water and energy access. In general, it is very expensive assembly power systems for far away rural areas. Thus, other strategies, such as stand alone microgrids supplied by photo-

voltaic panels associated with battery banks can be economically viable. In contrast with other energy technologies, in stand alone application, the solar energy production is only limited by the installation cost and the battery banks used, due to intermittency over time (Pihl et al, 2012).

With this challenge, this work proposes the creation of an autonomous electrocoagulation system (AES), with topology presented in Fig. 1.2.
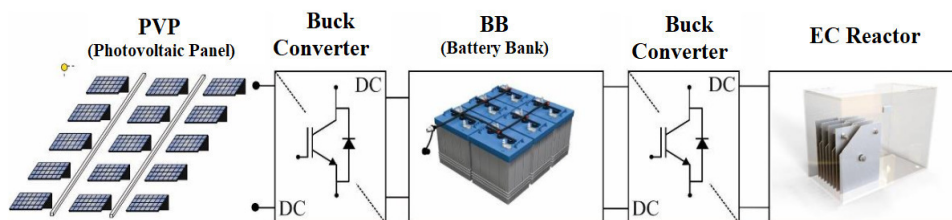
Figura 1.2: Scheme of the AES.

1.1   Electrocoagulation Process

In several academic works, it has been demonstrated the effectiveness of the set electrocoagulator - photovoltaic system (EC-PS) as an alternative to treat different types of wastewater. Among the studies, (Valero et al, 2008) proposed a versatile EC-PS arrangement, where the treated effluent flow is dependent on the local irradiance conditions, emphasizing the importance of the photovoltaic arrangement configuration, which must be determined for each type of water to be treated. (Marmanis et al, 2015; Pirkarami et al, 2013) studied the effect of different variables such as water conductivity and solar irradiation conditions on the removal of pollutants from the water. (Hussin et al, 2017) studied the performance of the EC-PS set under different meteorological conditions considering the assembly operating costs.

In many developed countries, centralized large-scale water treatment facilities are adequate and highly profitable. However, even in these countries, there are numerous situations in which smaller localized water treatment facilities are preferable to centralized treatment. Alternatives that offer ad-

vantages in terms of process automation and cost have been studied. Between these technologies, the electrocoagulation process has standing out as a promising technology in water treatment (Holt et al, 2005). In this purpose, other studies explore the operational parameters such as conductivity, current intensity, electrolysis time and pH (Ulu et al, 2014; Kourdali et al, 2014), and also there are researches exploring with the coagulation mechanisms (Dubrawski and Mohseni, 2013; Harif et al, 2012), and using synthetically water samples to simulate high concentration of natural organic material (Yıldız et al, 2008; Yildiz et al, 2007).

1.2   Energy Process: BB and PVP

A fundamental component for an integration between a system powered by a photovoltaic panel (PVP) is the battery bank (BB). The intermittent form of the solar irradiance causes variations in the energy system transferred by the PV (Villalva, 2010). Faced with this problem, it is usual to use a battery bank in cascade with photovoltaic solar energy to guarantee the moments of lack of solar energy, transfering energy to the existing load (Alvarez-Guerra et al, 2011).

Batteries are electrical energy storage devices, in the form of chemical bonds of their components. Generally the batteries operate using the chemical process of oxidation and reduction. Batteries can be classified between flow and secondary batteries, where the flow are those that have two tanks for electrolytic storage, positive and negative and have a higher density of energy and power, while the secondary ones have the capacity to be recharged when injected a current opposite their terminals. Among the secondary, ones a type stands out, due to its characteristics of operation and durability (Stroe, 2014; Schonberge, 2010).

In this way, in autonomous systems the quality of the operant battery is fundamental, since it is expected a reduced number of maintenance and highest quality in the parameters operation. The applicability of the lithium ion battery in this context, is the choose of this work, make it appropriate. Lithium-ion batteries have become in the last years one of the most popular energy storage technology for wide applications (Stroe, 2014). The cathode

of this battery is a compound of lithium and cobalt oxide, and the anode is carbon, and these two electrodes being separated by a non-conducting electrolyte. Their operating principle is based on the redox reactions in electrochemical cells. In this context, the advantages and disadvantages of this type of battery in the system can be listed as follows (Stroe, 2014; Chen and Rincon-Mora, 2006):

- Highest efficiencies among the electrochemical energy storage technologies;

- Long calendar and cycling lifetime;

- Low self-discharge rate;

- High cost compensated with the safety(in any cases);

According to (Stroe, 2014) the Li-ion batteries are suitable candidates for most of the storage applications (especially for the short and medium voltage), when analyzing characteristics such as cycle lifetime, efficiency, environment, cost/cycle, and others. This information is summarized in Fig. 1.3. These technology stand out mainly in terms of life time and efficiency, as well as environmental factors.

1.3   System Integration: Buck Converters

Due the different operating voltage (PVP, BB and EC) and the inherent need of joint operation between them, necessary to properly couple between these through power electronic converters. The connection is made using buck converters, responsible for reducing the applied input voltage. For the proposed AES, two Buck converters were used, in the first stage the connection between the PVP and the BB, and in the second stage the connection between the BB and the EC.

Its practical use can be justified, due to its enormous applicability, to loads of several voltage levels, such as: traction control of motors in automobiles, marine cranes, conveyors in mines, among others (Rashid, July 29,

Requirements	Energy storage technologies											
	VRB	PSB	ZnBr	ZnAir	Supercap	SMES	Flywheel	Lead	NiCd	NaS	NaNiCl	Li-ion
Response time	+	+	+		++	++	++	++	++	++	+	++
Discharge time	++	++	++	++	-	-	+	++	++	++	++	++
Cycle lifetime	++	-	+	++	++	++	++	-	+	+	+	++
Calendar	+	+	-	+	++	++	++	+	++	++	+	++
Self discharge	++	++	++	++	-	-	-	++	++	+	+	++
Efficiency	+	-	+	-	++	++	++	+	-	++	+	++
Environment	++	-	+	+	++	+	++	+	-	++	++	++
Maturity	+	-	+	-	+	-	+	++	++	+	+	+
Demonstration in MW	+	-	+	-	-	+	+	+	-	++	-	++
Cost/cycle	+				-			+	-	-	+		+

Figura 1.3: Comparison between different types of batteries (Stroe, 2014).

2013). They provide smooth throttle control, high efficiency and fast dynamic response. This converter has an average output voltage lower than the input voltage (Barbi, 2015). With the control of the switch in the converter it is possible to obtain two modes of operation: discontinuous and continuous mode. The latter was chosen for the development of this work, because it is necessary regulating the voltage in charge through a capacitor.

1.4   Objectives

Due to the wide range of electrocoagulation system integrated in the literature, the objective of this work is to analyze the integration between the PVP, BB and the EC and propose an autonomous system to possibility an independent process of clarification. The optimization of different operational variables when using the EC associated with PVP systems is analyzes to develop a high efficiency and reliability converter. Moreover, there is a lack of knowledge in the literature related with the design of PV systems integrated with electrocoagulator reactors and this was one of the reasons to motivate the present study.

In this context, this work intends to analyze the autonomous system with the following contributions:

- Adapt the EC to a PVP and determine methodologies for the integration between the AES components;

- Modeling of the two bucks converters used in system integration and to control the relevant variables, such as PVP voltage and electrocoagulator current;

- Analyze the implementation of a perturb and observes (P&O) type algorithm to extract the maximum power from the PVP;

- Analyze the power losses due to the presence of electronic switches in the converters.

1.5   Text Organization

This work is divided in five chapters. In the first chapter a contextualization is performed about autonomous system proposed and about the elements present in the system, addressing some of its characteristics, motivations of use and mode of integration. In the second chapter, a theoretical review is made on the buck converter control, MPPT, PVP, Li-ion battery cells models and thermal models used to simulated and others relevant concepts. In the third chapter, the study cases are presented in order to analyze the control, MPPT, power losses and operation points. In the fourth chapter is presented the simulation results. Finally, the fifth chapter presents the conclusions obtained in this work.

Literature Review

In this chapter, a theoretical review of the most relevant concepts of buck converters, PVP models, control design, modulation, MPPT and Li-ion batteries models are presented.

2.1   PVP, BB and EC Integration

The PVP is connected in cascaded with a battery bank by means of a c.c./c.c buck converter (identified as buck 1). The BB, in turn, is cascaded with the EC system, through another buck converter (identified as buck 2). For representative effects, the electrocoagulator is indicated as a variable resistance R, as usually in the literature (Mollaha et al, 2004; Dubrawski and Mohseni, 2013; Harif et al, 2012). However, this resistance depends on the chemistry composition of water, thus, for simulation purposes the use of a fixed resistance does not significantly affect the study of the other elements.

The buck converter 1 must make the connection between the PVP and the BB, reducing the panel maximum voltage to V_{bat}, defined as the battery voltage. The operation of the buck converter circuit can be divided into two modes, depending on the driving condition of the switch (IGBT). In operation mode 1, when the switch is closed, the input source is responsible for charging all the rest of the circuit. The operation mode 2, occurs when the switch is open, and in this case the output current of the inductor is responsible for feeding the load and the capacitor.

Considering a maximum power voltage of V_{mp} and an output voltage of

$V_o = V_{bat}$, the duty cycle value ($d = \frac{V_o}{V_{mp}}$) is obtained. With the values of the converter components and d, it is possible to obtain the critical inductance values L_{crit} and capacitance C_{crit} (Rashid, July 29, 2013), responsible to operate the converter in the continuous mode, defined as:

$$C_{crit} = \frac{1-d}{16Lf^2} \tag{2.1}$$

$$L_{crit} = \frac{(1-d)R}{2f} \tag{2.2}$$

The integration between the buck converters 1 and 2 with the other AES components are show in the Fig. 2.1. The signal d_1 is the output of the control used in the IGBT 1, with two loops, the inner one being responsible to control the inductor converter 1 and the outer loop of the panel output voltage. Instead in the IGBT 2, d_2 is carried out the control of the inductor current of the converter 2.
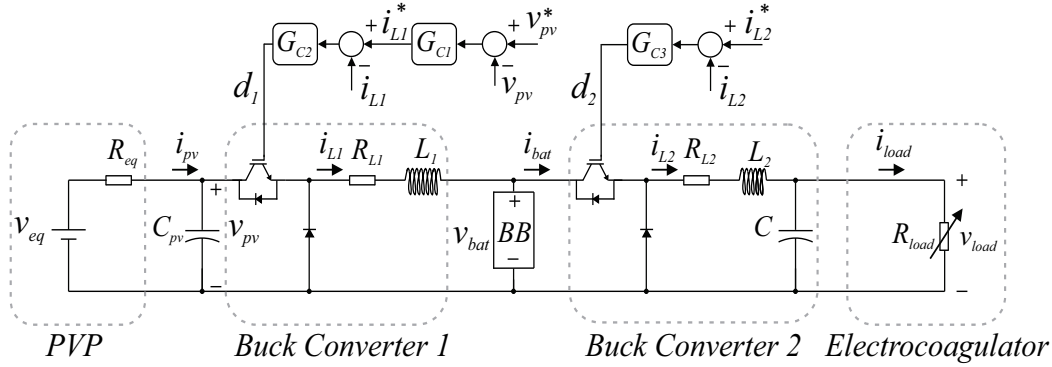

Figura 2.1: Stage of connection between PVP, BB and EC.

2.2   PVP Model

Regardless of the nature of the autonomous PS, it is extract the maximum power supplied by the PV array. In general, it is applied perturb and observe algorithm (P&O) and control methods to obtain the maximum power available (Prieb and Massen, 2011). One of the main problems, for

this energy transfer, is that the equivalent model of the down converter fed by a PS is dependent on the equivalent PS serial resistance, which varies according to the incident solar irradiance, and directly interferes in the output voltage of the panel, by ohm law. One option for solving this equivalent resistance variation problem is the insertion of an input capacitor. In spite of solving the problem, this option brings one head problem: the system cost increase. Thus, the converter lifetime can be reduced (Sera et al, 2007). In other hand, has the intention of regulating the output current of the panel, so that it does not present a switched characteristic in current, due to the operation of the buck.

In spite of the inherent limitations of a PV connected to different loads, the representation of this one for simulation purposes is very important, in order to obtain the output voltage and current, characteristic MPPT operating points, transferred power, P&O efficiency, among others. To simulation propose, the panel model used in this work was proposed by (Nguyen and Lehman, 2008). The basic equation that describe the output current of the PV is modeled by equation (2.3).

The modeling equations of the panel are of non-linear characteristics, since it involves multiplication of variant terms in time. Thus, it becomes necessary to linearize the model. Then the small signal analysis method is used. The first step of this method is to generate a small disturbance in a steady state and to verify what happens in the system. In this case, the solar cells utilized have a characteristic series R_S and parallel R_P equivalent resistance (Villalva et al, 2009),(Nguyen and Lehman, 2008).

$$I = I_{PV} - I_O \left[exp \left(\frac{V + R_S I}{V_t m} \right) - 1 \right] - \frac{V + R_s I}{R_{pm}} \qquad (2.3)$$

where the value of I_{PV}, I_0 and V_t are defined as:

$$I_{PV} = [I_{PVn} + K_I(T - T_N)] \frac{G}{G_N}, \qquad (2.4)$$

where I_{PVn} is the photoelectric current at rated conditions (generally $T_N = 298$ K and $G_N = 1000 W/m^2$), T operating temperature, G the solar radiation on the surface of the device and K_I is the constant that relates the variation

of the current as a function of temperature,

$$I_0 = \frac{I_{sc,n} + K_I(T - T_N)}{exp(\frac{V_{oc,n} + K_V(T-T_N)}{aV_t}) - 1},$$ (2.5)

where K_V and K_I are the voltage/temperature and current/temperature coefficients, $I_{sc,n}$ is the short circuit current, a is the constant of diode ideality, between $1 \leq a \leq 1.5$, and V_t is the thermal voltage defined as:

$$V_t = \frac{N_S kT}{q},$$ (2.6)

on panel with N_S and N_P cells connected in series and parallel, respectively and k is the Boltzmann constant ($1.3806503.10^{-23}\ J/K$).

The model of the simulated PVP is show in the Fig. 2.2.
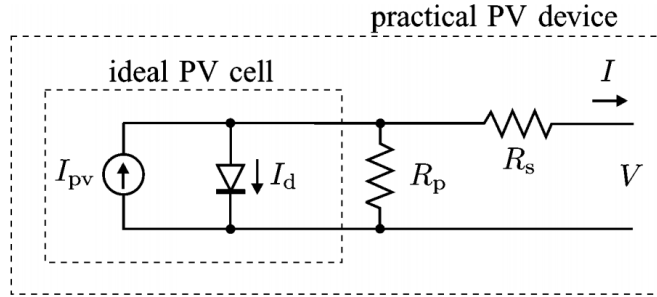
Figura 2.2: Simulated photovoltaic panel model (Villalva et al, 2009).

From the number of cells in series N_S used in the PV it is possible to increase the panel voltage. With the use of N_P cells in parallel, it is possible to increase the current capability. The characteristic curve I X V of the PV practical is shown in Fig. 2.3.

It is possible to see three important points in the PV curve: open circuit($V_{OC}, 0$), short circuit($0, I_{SC}$) and maximum power (V_{MP}, I_{MP}).

Figura 2.3: The characteristic curve I X V of the PV (Villalva et al, 2009).
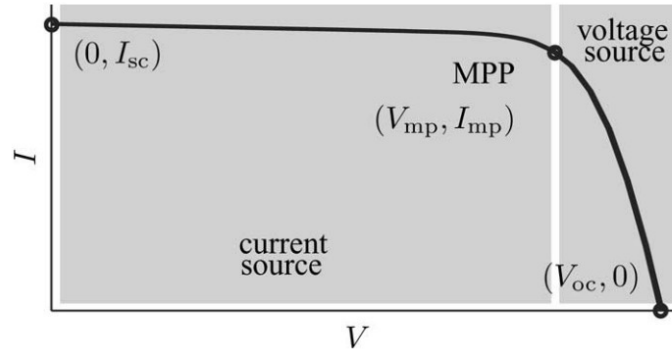
2.3   Li-ion Battery Model

Batteries are components responsible for energy storage and provide greater reliability and autonomy in the systems. The system proposed in this work uses lithium-ion (Li-ion) batteries. Due to the studies necessary to evaluate the power dissipation capacity, runtime, state of charge, among others, the modeling of this element for simulation purposes becomes a powerful tool for analyzing the battery response characteristics. In some electronic design automation (EDA), the equivalent circuits of different levels of abstraction, to apply, are usually obtained from bench tests, and seek to extract important information such as resistance and capacitance characteristics of the battery.

Accordingly researchers around the world have developed a wide variety of models with varying degrees of complexity. In special, the model of equivalent electrical circuit (EEC), used in this work, present the best results when compared to other models, such as the electrochemical models (Stroe, 2014; Gao et al, 2002).

In order to study the dynamics of this component is necessary to create virtual models. In this context, engineers and physicists study and develop the performance of different control strategies and circuits in a simulation, using PLECS software, for instance, then is used to simulated the system proposed in this work. It is possible to lift battery models through bench tests and from this with operating curves is made a model with capacitance, resistance and voltage inserted in a lookup table. The disadvantages of use

this model is the restrict point of operation, than the simulation can not extrapolate the test conditions (Chen and Rincon-Mora, 2006).
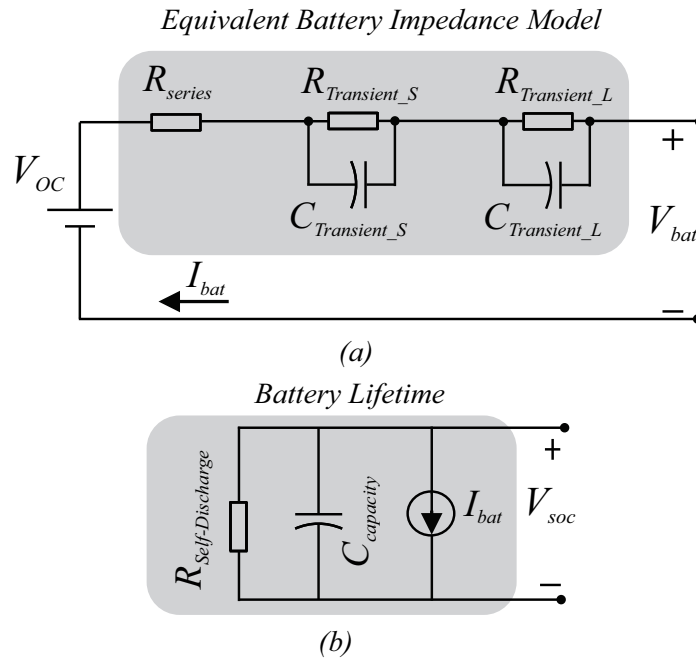

Figura 2.4: Schematic representation of EEC (a) Equivalent Battery Impedance Model (b) Battery Lifetime (Chen and Rincon-Mora, 2006).

To optimize the overall system performance, the I-V characteristics of the battery must be considered in differents conditions. Thus, the RC chain based electrical Li-ion cell models can be used to benchmark different charging and State of Charge (SOC) estimation algorithms.

The EEC model employed has variable capacitance and resistance that depend on its SOC. The RC network simulates the transient response, and depending on the technology employed, it can a larger number of RC in series. The open circuit voltage configures the standard output voltage of the battery, specified by the manufacturer and dependent on the SOC. In this way a voltage-controlled source is used. The proposed model capturing the dynamic electrical characteristics of batteries: usable capacity (Capacity), open-circuit voltage (V_{OC}), and transient response (RC network).

According to Fig. 2.4 (a), the circuit elements can be defined by the

following equations for the characteristic voltage battery model outlined in Fig. 2.5 (b). The Eqs. (2.7) to (2.12) express variable elements that are derived from bench tests and experimentally raised according to the SOC and the time running.

The open circuit voltage source is given by:

$$V_{OC} = -1.031e^{-35SOC} + 3.685 + 0.2156SOC - 0.1178SOC^2 + 0.3201SOC^3 \tag{2.7}$$

The resistances are expressed by:

$$R_{Series}(SOC) = -0.1562e^{-24.37SOC} + 0.07446 \tag{2.8}$$

$$R_{Transient\_S}(SOC) = 0.3208e^{-29.14SOC} + 0.04669 \tag{2.9}$$

$$R_{Transient\_L}(SOC) = 6.603e^{-155.2SOC} + 0.04984 \tag{2.10}$$

The capacitances are expressed by:

$$C_{Transient\_S}(SOC) = -752.9e^{-13.51SOC} + 703.6 \tag{2.11}$$

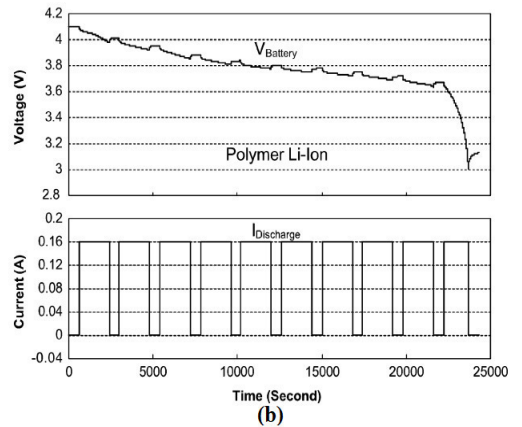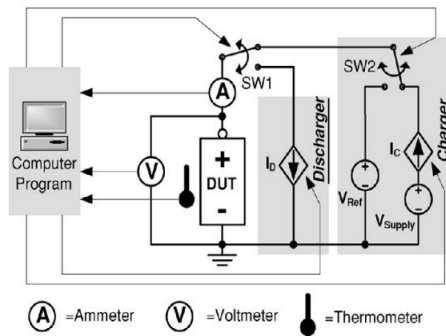$$C_{Transient\_L}(SOC) = -6056e^{-27.12SOC} + 4475 \tag{2.12}$$

Figura 2.5: (a) Battery test system. (b) Typical voltage response curve with pulse discharge current (Chen and Rincon-Mora, 2006).

The phenomenon of the usable capacity, SOC, can be modeled by a full-capacity capacitor ($C_{Capacity}$), a self-discharge resistor ($R_{Self-Discharge}$), and an battery current (I_{bat}), according Fig. 2.4 (b).

To extract all the parameters in the proposed model, a battery test system and an experimental procedure were designed to measure batteries conveniently and efficiently in Fig. 2.5 (a). The battery test system, includes a charge circuit, a discharge circuit, and a computer program. A switch SW1, is used to switch between the charge and discharge circuits. In the charge circuit, switch SW2 is used to switch to implement constant current charge for batteries. At the same time, the computer program monitors battery temperature and samples battery voltage and current once per second to obtain charge and discharge curves. Fig. 2.5 (b) shows a typical discharge curve with 160 mA pulse current on a polymer Li-ion battery. The pulsewidth is chosen to guarantee enough "hump" for sufficient data points and the off time is selected to allow the battery voltage to reach steady-state conditions. Finally, all the model parameters are extracted from these experimental curves.

2.4 Control Design and Buck Converters

The analysis of the control design was done by separating two stages present in the system: buck converter 1 and 2. The converters are modeled by the small signal analysis method, according (Barbi, 2015).

2.4.1 Converter 1 - PVP + BB

The implementation of the MPPT algorithm occurs at the buck 1 stage. The inner and outer loop controllers act together with the MPPT and are responsible for keeping the reference indicated by the algorithm (Sera et al, 2013).The buck converter 1 connects the PVP to BB and it is shown in Fig. 2.6.

In order to carry out the control of the inductor current and the voltage in the dc bus, two control loops are implemented. Fig. 2.7 shows the control configuration of the system, with the PI controllers G_{C1}(s) and G_{C2}(s),
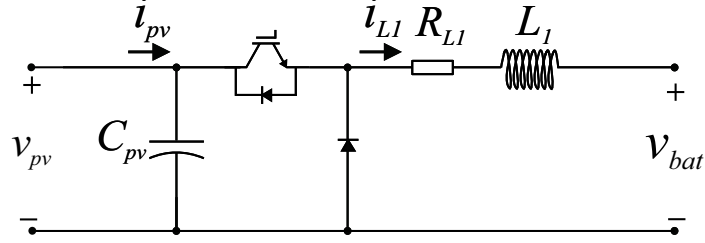
Figura 2.6: Converter Buck 1.

composed of an outer loop, tuned to control the PV voltage v_{pv}, and by an inner loop, tuned to control the inductor current i_{L1}.
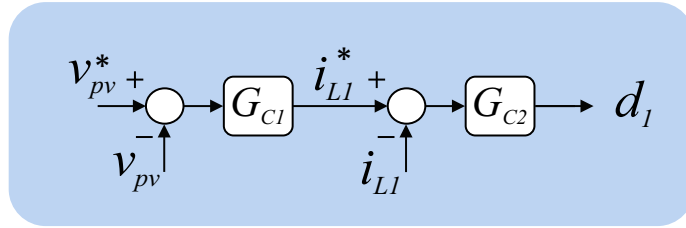
Figura 2.7: Control loop for panel voltage.

For modeling the buck converter, the PVP is linearized around the point of maximum power, thus being represented by a voltage source V_{eq} and a resistance R_{eq}. The cascade control loop, resulted in the following transfer functions.

$$\frac{i_{L1}(s)}{d_1(s)} = \frac{(C_{pv}v_{bat}d_1R_{eq}^2 + C_{pv}R_{L1}v_{eq}R_{eq})s + 2v_{bat}d_1R_{eq} - v_{eq}d_1^2R_{eq} + R_{L1}v_{eq}}{(d_1^2R_{eq} + R_{L1})[C_{pv}L_1R_{eq}s^2 + (C_{pv}R_{L1}R_{eq} + L_1)s + d_1^2R_{eq} + R_{L1}]}$$
(2.13)

$$\frac{v_{pv}(s)}{d_1(s)} = \frac{-R_{eq}[(d_1L_1v_{eq} - L_1v_{bat})s + (d_1^2R_{eq}v_{bat} - R_{L1}v_{bat} + 2d_1R_{L1}v_{eq})]}{(d_1^2R_{eq} + R_{L1})[C_{pv}L_1R_{eq}s^2 + (C_{pv}R_{L1}R_{eq} + L_1)s + d_1^2R_{eq} + R_{L1}]}$$
(2.14)

It is observed that these equations relate the current and the voltage with the duty cycle (d_1) ratio. Using Equations (2.13) and (2.14) it is possible to obtain the relation between the output voltage of the PVP and the inductor current.

Eqs. (2.13) and (2.14) can be simplified in terms of constants. The new constants (2.15), (2.16), (2.17) and (2.18) are in function of the parameters of resistance, inductance and capacitance of the converter. Besides the value of the battery voltage, the PV panel output voltage and duty cycle, (Padhi, 2010; Gayvoronskiy et al, 2017) are used to specify the gains of the controllers. Thus, equation (2.19) expresses the relation between the v_{pv} and i_{L1}, as a result of the ratio between Eqs. (2.13) and (2.14).

$$a = C_{pv}v_{bat}d_1R_{eq}^2 + C_{pv}R_{L1}v_{eq}R_{eq} \tag{2.15}$$

$$a' = -R_{eq}(d_1L_1v_{eq} - L_1v_{bat}) \tag{2.16}$$

$$b = 2v_{bat}d_1R_{eq} - v_{eq}d_1^2R_{eq} + R_{L1}v_{eq} \tag{2.17}$$

$$b' = -R_{eq}(d_1^2R_{eq}v_{bat} - R_{L1}v_{bat} + 2d_1R_{L1}v_{eq}) \tag{2.18}$$

$$\frac{v_{pv}(s)}{i_{L1}(s)} = \frac{a's + b'}{as + b} \tag{2.19}$$

The input voltage of the buck converter 1 depends on the level of incident irradiance. Thus, it is desired to obtain from the PV panel the best performance for a distinct irradiance profile, directly varying the cyclic ratio of the converter.

When cascade control strategies are designed, the most important consideration is that the inner loop should respond more quickly than the outer loop (Smith and Corripio, 2008). With the use of a controller in the inner loop, it was obtained a transfer function for closed loop with a 3rd order characteristic equation. In order to facilitate the controller design, it is possible

to reduce this equation to a 2nd order transfer function, considering the most significant pole.

In order to obtain the controller gains G_{C1} (K_{P1} and K_{I1}) and G_{C2} (K_{P2} and K_{I2}), the method of pole allocation is used. This method consists in allocating two real poles in the closed-loop transfer function, positioning one near the pole of the plant transfer function, defined as p_{MA} and the other pole n times greater than the first one, defined as np_{MA}. In the case of a second-order transfer function, the most significant pole is chosen. For this method, after defining the closed-loop poles of the controlled system, it is possible to improve and accelerate the response by varying both poles by a multiplicative factor n', moving both poles over the left half-plane axis (Padhi, 2010).

The new system is modeled by taking the new second-order poles, given by the characteristic closed-loop equation, is given by:

$$\frac{H'}{(s - n'p_{MA})(s - n'np_{MA})} = \frac{G_c(s)H}{1 + G_c(s)H} \ , \qquad (2.20)$$

where G_c and H represent the transfer functions of the controllers and the system, respectively, while H' corresponds to the numerator of the transfer function H. The values of K_P and K_I, to the inner and outer loop, are derived from the equality between the denominators of equation (2.20).

Similarly, for the outer loop, a smaller n pole of the significant pole of the outer loop was chosen, without significantly changing its position on the axis. Thus, the inner loop continues to be faster. The values are adjusted according to the need of the project. In order to simplify the analysis of the outer loop, it was considered that the inner loop was already controlled. The values of K_{P1} and K_{I1} of the inner loop of the buck converter 1 can be found by:

$$K_{P1} = \frac{(1 - n'_1(1 + n_1))(mcd - e)}{b} - \frac{acd}{b^2}(\frac{e - mcd}{cd})^2 n'^2_1 n_1 \qquad (2.21)$$

$$K_{I1} = \frac{cd}{b^2}(\frac{e - mcd}{cd})^2 n_1'^2 n_1 \qquad (2.22)$$

where m, c, d and e is defined respectively by:

$$m = \sqrt{(\frac{e}{cd})^2 - \frac{4}{d}} \qquad (2.23)$$

$$c = C_{pv}^2 R_{eq} + R_{L1} \qquad (2.24)$$

$$d = C_{pv} L_1 R_{eq} \qquad (2.25)$$

$$e = C_{pv} R_{L1} R_{eq} + L_1 \qquad (2.26)$$

if m contains an imaginary part, adopting $m = 0$ for the purpose of calculating the gains. The values of K_{P2} and K_{I2} of the outer loop of the buck converter 1 can be found according to equations (2.27) and (2.28).

$$K_{P2} = bn_2'(1 + n_2) - b - \frac{b^2 n_2'^2 n_2 a'}{b'a} \qquad (2.27)$$

$$K_{I2} = \frac{b^2 n_2'^2 n_2}{b'^2 a} \qquad (2.28)$$

The constants expressed in equations that specify controller gains are in function of the converter parameters, such as resistance, inductance and capacitance, also the value of the battery voltage, the photovoltaic output voltage and duty cycle are used to specify the gains of the controllers.

In order to illustrate the method of pole allocation, a simple example was made. Considering a transfer function with numerator $H' = 1$, open-loop pole $p_{MA} = 100$ and a gains controller, $K_P = 10$ and $K_I = 1$. In this way, the bode diagram of this function was analyzed, given by the right-hand portion of the equation (2.20). Fig. 2.8 shows the frequency response, in magnitude

and phase, with different gains of p_{MA} and is indicated the original transfer function.

To obtain the equality expressed in the equation, the gains n and n' were adjusted, in order to approximate the maximum frequency response, in order to validate the gains projected by the methods. Analyzing the bode diagram, it is verified that for $n = 0.01$ and $n' = 1$, the answer approximates satisfactorily the original transference function.
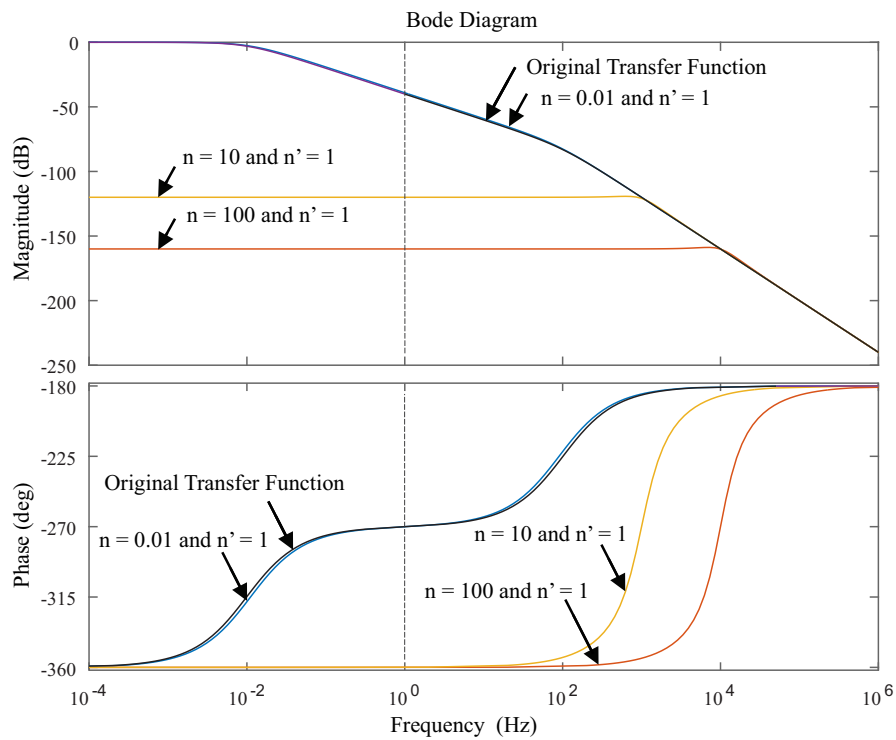

Figura 2.8: Bode Diagram.

In particular, it is necessary to emphasize that as the system operates in c.c. mode. Due to frequency proximity of 0 Hz, the 1 Hz point has been highlighted. It is possible to verify the difference, for low frequencies, between the responses in magnitude, in specially, and phase of the system for different gains used, n and n'.

2.4.2   Converter 2 - BB + EC

The buck converter 2 is responsible to connect the BB with the EC. The buck converter 2 is shown in Fig. 2.9.
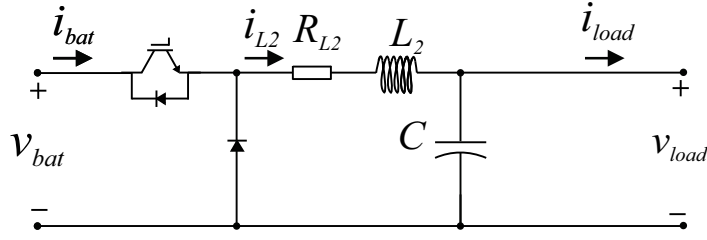

Figura 2.9: Converter Buck 2.

The buck converter 2 is controlled in current mode. The control loop is shown in Fig. 2.10, resulting in the transfer function shown in equation (2.29). In the modeling design, a simplification is considered, once the output capacitor C is sufficiently large.

$$\frac{i_{L2}(s)}{d_2(s)} = \frac{V_{bat}}{L_2 s + R_{L2}}. \tag{2.29}$$

It is observed that (2.29) relates the current in the inductor with the duty cycle ratio applied in the switch. It is known that the current used in electrocoagulation will determine the amount of metal that will be oxidized at the anode (Mollah et al, 2001). Thus, some cares should be taken when choosing the value of the reference current, since it can mean loss of power by Joule effect, and also a higher frequency of maintenance of the electrodes (Dubrawski and Mohseni, 2013; Mollaha et al, 2004). In this way, the electric current is identified as the main operational parameter of the electrocoagulation process, affecting not only the system response time, but also strongly influencing the separation and removal of pollutants (Mollah et al, 2001).

The values of K_{P3} and K_{I3} can be found according to:

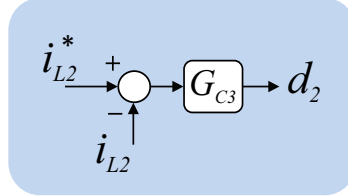$$K_{P3} = \frac{R_{L2}(n_3'(1 + n_3) - 1)}{V_{bat}} \tag{2.30}$$

Figura 2.10: Control loop for current in the EC.

$$K_{I3} = \frac{n_3'^2 n_3 R_{L2}^2}{V_{bat} L^2} \qquad (2.31)$$

The constants expressed are in function of the converter parameters such as of resistance, inductance and capacitance. Also, the value of the electro-coagulator resistance and the converter output capacitance and duty cycle (d_2), according to (Barbi, 2015).

2.4.3   Modulation Technique

A widely used technique in converting voltage levels is pulse width modulation (PWM), which consists of comparing two signals of a single-phase pulse width, voltage, one of low frequency (reference) and the other of high frequency (carrier), resulting in an alternating signal with fixed frequency and variable pulse width.

The PWM modulation technique involves important factors, such as, identified in the Fig. 2.11:

- Reference Signal: To obtain a signal at the output of the converter, it is necessary to compare it with a voltage signal, called reference signal, which is equal to the desired output voltage. In the c.c./c.c. converter, the reference is a continuous voltage signal.

- Carrier Signal: It is a high frequency signal, responsible for setting the switching frequency and duty cycle. It should be at least 2 times larger than the reference signal (Nyquist's Theorem). This signal is responsible for the switching frequency of the switches (semiconductors). In
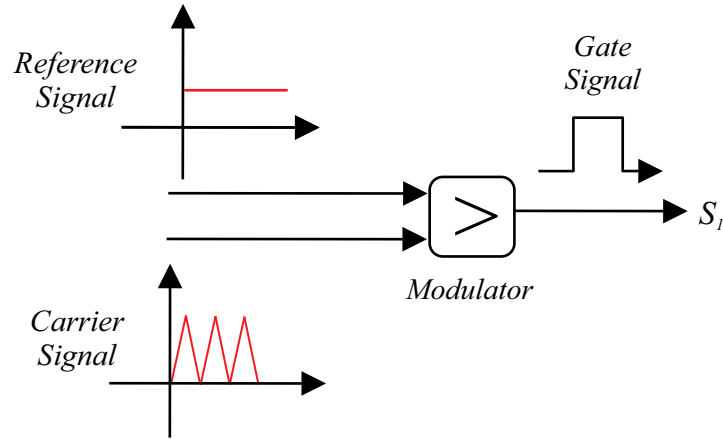
Figura 2.11: PWM Modulation Technique.

c.c./c.c converters, a triangular signal is used as the carrier.

- Modulator: It is the circuit responsible in comparing the reference signal with the carrier. The pulse width at the output of the modulator varies according to the amplitude of the reference signal compared to the carrier signal

2.5   Electrocoagulator

In the electrocoagulation process, the electrolytic reactor has sacrificial electrodes, which release chemical species acting as coagulants. When an electric potential is applied, the anode undergoes corrosion due to oxidation. At the same time, due to the applied potential, hydrogen micro bubbles can be formed at the reactor cathode by reduction reactions. These micro bubbles promote the separation of the residual particles by means of flotation (Chen, 2004). Thus, EC is a technique that can support the water treatment (clarification process) associated with the use of renewable energy sources.

Coagulant concentration is an important variable in electrocoagulation process. Generally, the aluminum concentration is the material used in the water treatment. The Faraday law described by:

$$m_{coag} = \frac{\phi M t i_{load}}{zF} \tag{2.32}$$

can be used to link the metal mass generated by the electrolytic system considering the current intensity i_{load} and the electrolysis time t, in seconds. M is the metal atomic weight, z is the number of electrons transferred in the anodic dissolution, 3 for aluminum, F is the Faraday constant (96.486 C/mol) and ϕ is the current efficiency, which depends on the specific characteristics of the experimental set-up and the raw water quality (Dubrawski and Mohseni, 2013; Combatt et al, 2017).

There are several combinations of current intensity and electrolysis time that will dissolve the same mass of aluminum m. Besides, must be consider the water conductivity that will directly influence in the the current intensity and electrolytic time.

The monopolar electrodes, showed in Fig. 2.12, are arranged in series with other cells to increase the system operating capacity. According to (Combatt et al, 2017) the coagulation process will initiated by neutralizing the charges of the particles by released ions. The released ions remove undesirable contaminants either by chemical reaction and precipitation, or by causing the colloidal materials to coalesce, which can then be removed by flotation.
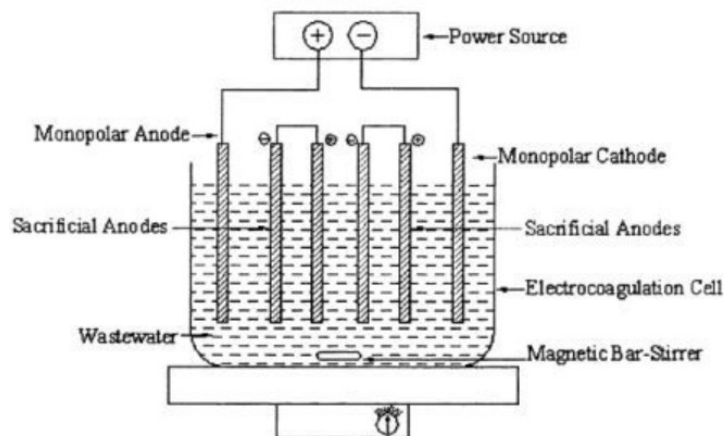

Figura 2.12: Monopolar Electrolytic Reactor (Mollah et al, 2001).

According to (Mollah et al, 2001) the advantages of EC can be listed as:

- Removes heavy metals as oxides that pass toxicity characteristic leaching procedure;

- Removes suspended and colloidal solids;

- Destroys and removes bacteria, viruses and cysts;

- Low power requirements and operating costs;

- Low maintenance;

2.6   Thermal Model

In order to compare the thermal behavior of the semiconductors in the buck converters, the thermal model of the IGBTs and diodes were included (Rinaldi, 2001). Through the datasheet available it was possible to enter values of switching losses (turn on and turn off), conduction losses and the thermal impedance considering the Foster model of the switch. Because the characteristics of the semiconductor switches, such as silicon carbide technology, some types of losses are negligible and are not provided by the component datasheet.

The equivalent thermal model diagram used to design the heat sink is shown in Fig. 2.13.

For the calculation of the heat sink thermal resistance, the circuit shown in Fig. 2.13 was considered. The junction temperature T_j of both IGBT and diode were "forced"to stabilize at a predefined value (Ma et al, 2016). Since only one heat sink is used for both types of components, the junction temperature (T_j) and the heat sink temperature (T_h) are the same. Thus, for the calculation of the heat sink-ambient resistance (R_{ha}), the junction temperature, heat sink temperature and ambient temperature were considered equal. For this it was necessary to eliminate the thermal dynamics (resistance and capacitance) of the IGBT and the diode. Thus, the power dissipated (P_{diss}) is obtained by means simulations in both components (Ma et al, 2016). After obtaining the dissipated power it was possible to calculate the value of the thermal resistance through in the equation (2.33).
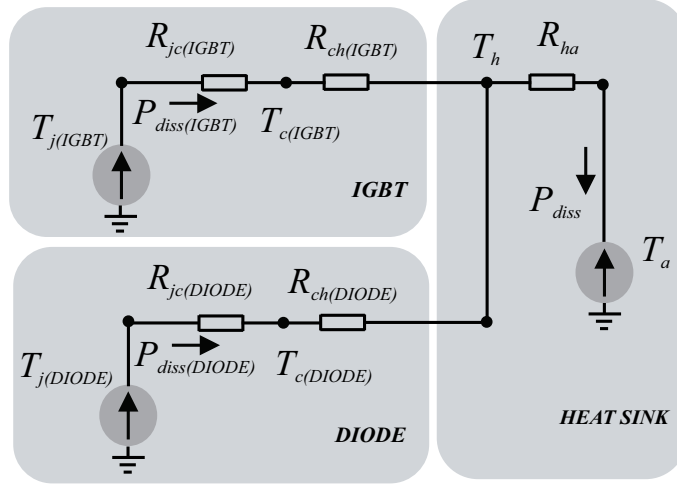
Figura 2.13: Thermal model diagram.

$$R_{ha} = \frac{Tj - Ta}{P_{diss}} \tag{2.33}$$

At $T_j = 313$ K, $T_a = 298$ K and $P_{diss} = 15.35$ W. This results in a thermal resistance of 0.977 K/W. For the calculation of the capacitance, an analysis is performed using the time constant $\tau = $ RC. For τ equal to 0.01 s, we have the value of the thermal capacitance equal to 0.00977 $\frac{Ks}{W}$.

2.7 MPPT Algoritm

Electronic converters operating in conjunction with PS have the inherent need to use a maximum power point tracking (MPPT), which is responsible for extracting the maximum power from the PVP (Prieb and Massen, 2011).

As the variations in the solar irradiance occur, it acts directly on the I X V operating curve of the PVP. In cases where the distribution of solar irradiance is irregular along the panels present, this distribution will make the implemented algorithm not valid for all panels, which reveals one of the challenges for the MPPT algorithms (Sera et al, 2006).

For the development of this work, the P&O algorithm was used, and its
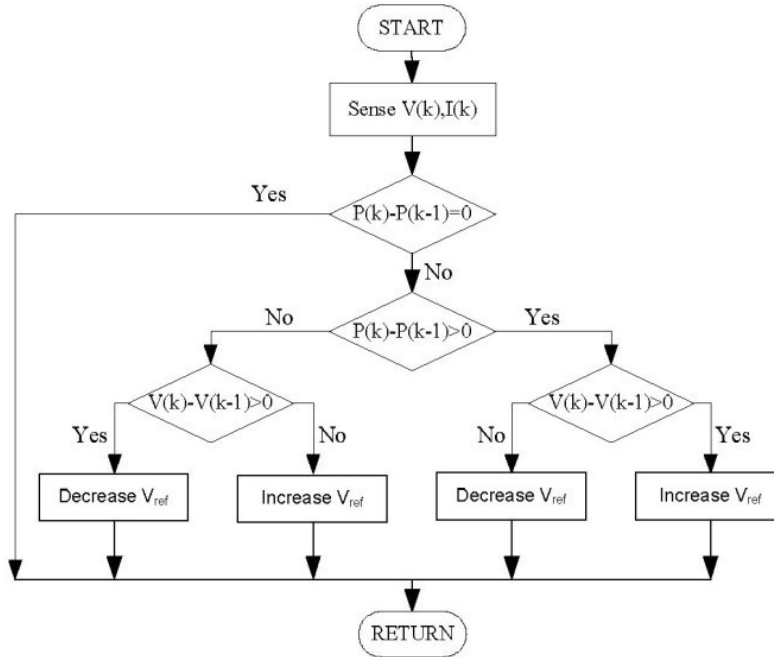
operation flowchart is shown in Fig. 2.14.

Figura 2.14: Flowchart of the P&O algorithm (Sera et al, 2006).

In its operation the algorithm periodically increases or decreases the voltage and compares the output power with its previous value, in case of power increase, the direction of the disturbance will continue in the same direction in the next cycle. In this way when the maximum power point is reached, the algorithm P&O will oscillate around it. The perturbation and observation method presented is one of the simplest among existing MPPT methods, and presents excellent operating performance, being easy to implement. Some more sophisticated methods are based on the same principle employed in the P&O method. Examples are the modified P&O technique, hill climbing, and modified hill climbing (Sera et al, 2006).

In order to analyze the effectiveness of the implemented MPPT algorithm, a study was made on its efficiency, using the definitions proposed by (Prieb and Massen, 2011; Sera et al, 2006; Ahmed et al, 2016), in which this analysis can be defined in two ways: the instantaneous efficiency, associated with situations where the solar irradiance remains constant during the test interval considered, and the dynamic efficiency of a MPPT, which con-

siders the moments of variation in the intensity of the resulting irradiance, for example, the passage of clouds, among others (Ahmed et al, 2016).

The equations (2.34) and (2.35) indicate the mathematical definition of dynamical and instantaneous efficiencies, respectively.

$$\eta_{MPPTdin} = 100 \int_0^{Tmm} \frac{P_{Pv_{meas}}}{P_{Pv_{ideals}}} \tag{2.34}$$

$$\eta_{MPPTins} = 100 \frac{P_{Pv_{meas}}}{P_{Pv_{ideals}}} \tag{2.35}$$

where Tmm is the time of irradiance solar variation.

Methodology

In this chapter, the simulation parameters, as well the methodology, applied to study the operation, availability and validity of the proposed AES are presented.

3.1 Simulation Parameters

The main parameters of the designed AES are presented in the following tables. Simulations were performed in PLECS environment aiming to make the analyzes at relevant points of study.

The PVP parameters used for the simulation are found in Tab. 3.1, while the BB parameters used for the simulation are found in Tab. 3.2.

The Buck converters 1 and 2 parameters used for the simulation are found in Tab. 3.3. The PI controllers, of both buck converters are discretized by Trapezoidal method. Also, it is used same modulation techniques studied in the section 2.7 in both converters.

From this assembly the duty cycle value of converter 1 is $d_1 = 0.3183$, for the PS maximum voltage. The designed value of L_1 and C_1 are found by specifying the critical values. In this case, how the both converters are equal components, results in $L_{crit} = 2.13 \ \mu H$ and $C_{crit} = 78.136 \ \mu F$, considering the operation in continuous mode (Rashid, July 29, 2013).

Parameters (by panel)	Symbol	Value
Maximum power PV (W)	P_{max}	320
Maximum power voltage PV (V)	V_{mp}	37.7
Maximum power current PV (A)	I_{mp}	8.49
Open circuit voltage (V)	V_{OC}	46
Short circuit current (A)	I_{SC}	8.98
Series Resistance (Ω)	R_S	0.2375
Parallel Resistance (Ω)	R_P	5043.63
Series Cells	N_S	72
Parallel Cells	N_P	1
Operation Temperature (K)	T	298

Tabela 3.1: Parameters of the PVP.

Parameters (by cell battery)	Symbol	Value
Open circuit voltage cell (V)	V_{oc}	4.1
Capacitance cell (mF)	C_{term}	6.5
Series Cells	N_S	3
Parallel Cells	N_P	4
Operation Temperature (K)	T	298
Inicial SOC	SOC_{ini}	0.8
Maximum SOC	SOC_{max}	0.97

Tabela 3.2: Parameters of the BB.

3.2   Dynamic Profiles Studied

In order to analyze the joint operation of the proposed AES system, different references were used for the system. Thus, for the solar panel, a variation in the irradiance incident on the PVP, and for the current of the buck 2 inductor was used a step profile to obtain different index of electrocoagulation level. The following explains the dynamics of profiles introduced.

Parameter of buck Converter 1 and 2	Symbol	Value
Switching frequency (kHz)	f_{sw}	16
Sample frequency (kHz)	f_s	32
Capacitor and inductor switching (mF/mH)	$C_{PV}/L_1 = L_2$	3.9/1
Buck resistor (Ω)	$R_{L1} = R_{L2}$	0.1
Gains of buck Converter 1		
Proportional gain of inner loop	K_{P1}	-7.757
Integral gain of inner loop	K_{I1}	-67.129
Proportional gain of external loop	K_{P2}	-11.773
Integral gain of external loop	K_{I2}	-551.36
Poles gains (n_1, n_1') of inner loop	n_1/n_1'	$-10/20$
Poles gains (n_2, n_2') of external loop	n_2/n_2'	2/200
Gains of buck Converter 2		
Proportional gain	K_{P3}	-4.995
Integral gain	K_{I3}	-66666.667
Poles gains (n_3, n_3')	n_3/n_3'	$2/-20$

Tabela 3.3: Parameters of the buck converters.

3.2.1 Case Study 1: Solar Irradiance Variations

An irradiance profile according to Fig. 3.1 was simulated. This can be described as follows:

- Irradiance starts at the level of $300W/m^2$ and at the instant t = 0.5s, thereafter it increases to a level of $500W/m^2$ over a growth rate of $2000(W/m^2)/s$. At time t = 1.5s, it rises above the same growth rate until the maximum solar irradiance of $1000W/m^2$. In this first stage, the reaction of the system to a profile of elevation of solar irradiance is studied.

- The irradiance starts from the $1000W/m^2$ level and later at time t = 3s it slopes to the level of $500W/m^2$ over a decrease rate of -2000 $(W/m^2)/s$. Later at time t = 4s, it decreases over the same rate until the minimum solar irradiance of $300W/m^2$ is reached. In this second stage, the reaction of the system to a profile of reduction of solar irradiance is studied.
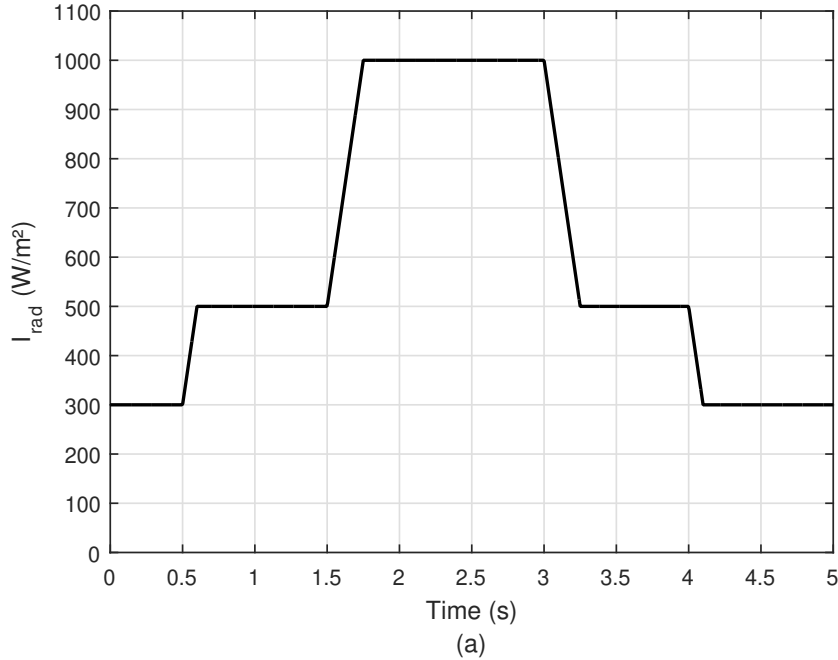
Figura 3.1: Solar Irradiance Dynamics

The irradiance profile introduced is mainly justified by the need to analyze the MPPT performance used and the projected control.

3.2.2 Case Study 2: Current Step in the Load

Simultaneously with the introduction of the solar radiation dynamics, reference steps were applied to the current in the inductor of the buck converter 2. The profile is analyzed below and shown in Fig. 3.2:

- Between the time t = 0s and t = 1.5s, a current step of 1A is used.

- Between the time t = 1.5s and t = 3.5s, a current step of 2A is used.

- Between the time t = 3.5s and t = 5s, a current step of 1.5A is used.

According to (Dubrawski and Mohseni, 2013; Combatt et al, 2017), the current value in the electrocoagulator is proportional to the rate of aluminum
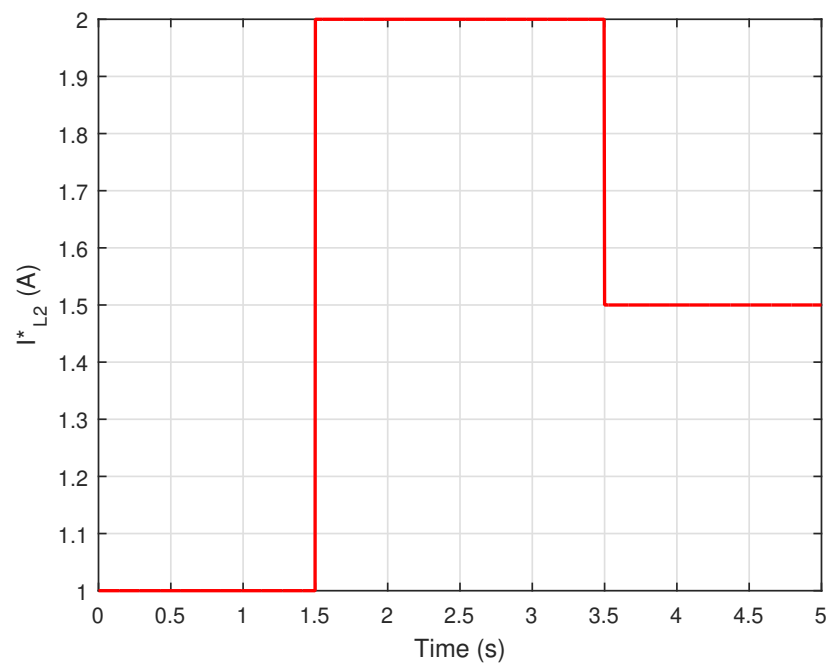
Figura 3.2: Reference Step Current in I_{L2}

concentration in the water, due to the release of these aluminum ions in the aqueous medium. In this way, the use of this profile is justified, in order to compare different rates of electrocoagulation.

3.3   Power Losses Analysis

In order to evaluate the power losses in the semiconductors devices, an analysis was made of the influence of solar irradiance and current step on switching losses (on and off), as well as on the conduction losses. The chosen IGBTs and diodes are of the silicon carbide technology. This technology of electronic switches reduce the losses to a small value when compared to the traditional ones of silicon. Therefore for the losses, especially of switching, it will be observed reduced values, or almost negligible.

3.3.1   Case Study 3: Power Losses Analysis - Solar Irradiance

In this study the analysis of different levels of solar irradiance on the losses of the IGBTs and diodes present in the converters were made. For this, the losses of the diodes present in both converters, as well as the IGBTs were joined. Different constant values of solar irradiance were used for the study, in which case the reference current of the buck converter 2 was given over 1 A for all time. The values of irradiance levels studied are:

- $I_{rad} = 100W/m^2$ and $I_{L2}^* = 1A$;

- $I_{rad} = 300W/m^2$ and $I_{L2}^* = 1A$;

- $I_{rad} = 500W/m^2$ and $I_{L2}^* = 1A$;

- $I_{rad} = 700W/m^2$ and $I_{L2}^* = 1A$;

- $I_{rad} = 1000W/m^2$ and $I_{L2}^* = 1A$.

3.3.2   Case Study 4: Power Losses Analysis - Current Step

Different constant current values were used in the buck converter 2 for the study, in which case the reference solar irradiance was given over $300W/m^2$ for all time. The following are the chain step values studied:

- $I_{L2}^* = 1A$ and $I_{rad} = 300W/m^2$;

- $I_{L2}^* = 1.5A$ and $I_{rad} = 300W/m^2$;

- $I_{L2}^* = 2A$ and $I_{rad} = 300W/m^2$;

- $I_{L2}^* = 2.5A$ and $I_{rad} = 300W/m^2$;

- $I_{L2}^* = 3A$ and $I_{rad} = 300W/m^2$.

3.3.3   Case Study 5: AES Efficiency

In order to perform a study on the efficiency of the AES, was calculated considering the following definition:

$$\eta_{sis} = \frac{P_{IN} - P_{losses}}{P_{IN}} \qquad (3.1)$$

where P_{IN} represents the input power of the system and P_{losses} the losses of conduction and switching of the semiconductors, in addition to the losses of the resistors of the converters.

3.4   Case Study 6: SOC and Battery Voltage Analysis

In order to perform a study on the battery SOC, a test was performed forcing the battery to discharge during a certain period. For this, an irradiance profile was used as shown in Fig. 3.3, where a maximum irradiance of

$300 \ W/m^2$ was used during the time from t $= 0$ s to t $= 1$ s, with a decrease of $20000 \ (W/m^2)/s$, with in all the rest of the time the panel receives no more solar irradiance until t $= 220$ s. The reference current in the buck used was $I_{L2}^* = 1A$, throughout the test.
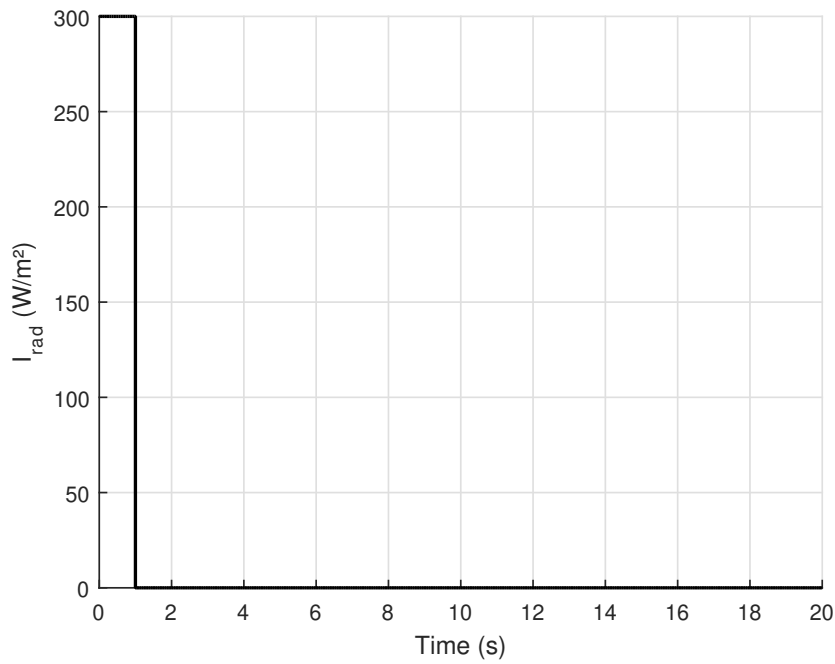

Figura 3.3: Solar Irradiance Dynamics

Results and Discussion

4.1 Dynamics Simulation

In this section the operating characteristics of the proposed AES are analyzed. For the joint use of the solar radiation profiles and current steps, the following results were obtained.

4.1.1 Circuit Characteristics

Fig. 4.1 (a) shows the dynamics of the irradiance profile and the Fig. 4.1 (b) shows the power supplied by the PVP, obtained by the characteristics of voltage and current terminal. It is observed that the panel obtained a acceptable efficiency, when compared with the incident irradiance, related to the ideal power to be developed. It is observed that the development of power by the panel in the ramps of growth of the solar irradiation, does not present linear characteristics according to the profile. For the slope ramps the exponential characteristics were observed.

The other characteristic observed was the battery voltage, using the model presented in this work. According to Fig. 4.2 it is possible to observe that the battery voltage followed the irradiation profile, being proportional its intensity level. The nominal voltage extrapolated to the maximum level of solar irradiance the initially projected 12 V, however the voltage is in a practical range practicable for real situation, validating the used battery model.
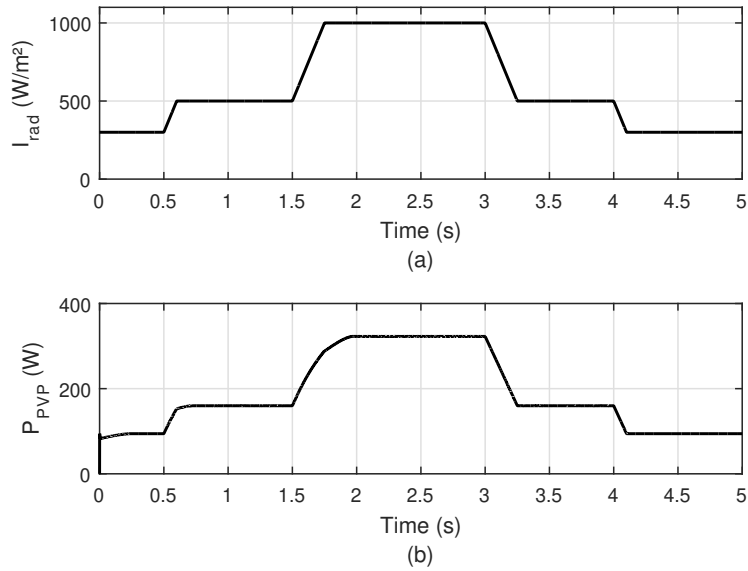
Figura 4.1: Irradiance and voltage characteristics of the PVP.
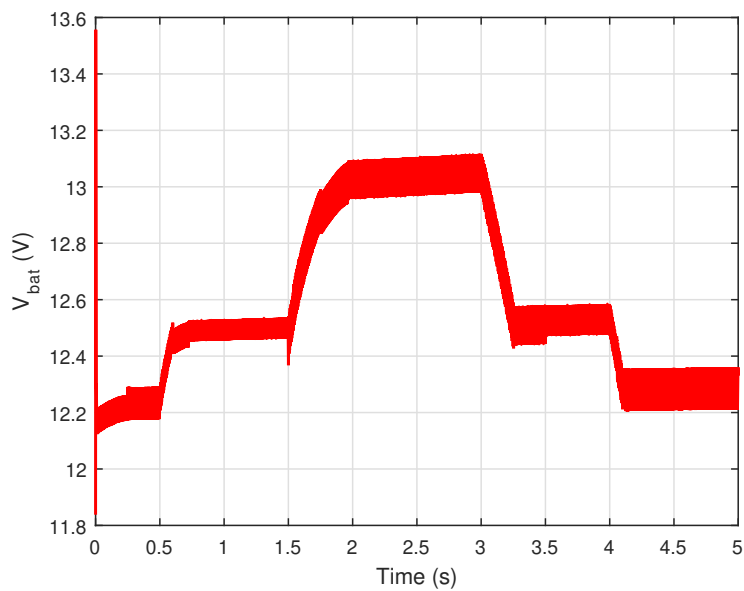(a) Irradiance profile inserted in the PVP. (B) Power developed by the panel.

Figura 4.2: Measured BB Voltage

4.1.2   Characteristics of Controls

Fig. 4.3 (a) and (b) show the currents in the inductors of the buck converters 1 and 2, respectively. The chains for both controllers presented a acceptable answer, in both permanent and transitional response. For Fig. 4.3 (b) three values of desired currents reference were used for the current in the inductor, 1 A, 1.5 A and 2 A, representing the adjustment for the operation of the electrocoagulator. In Fig. 4.4 the current was obtained at load R_{load}, which correlates directly with the voltage in the EC. This is a evidenced of good response and accommodation of the reference values, without undesirable oscillations and extrapolations.
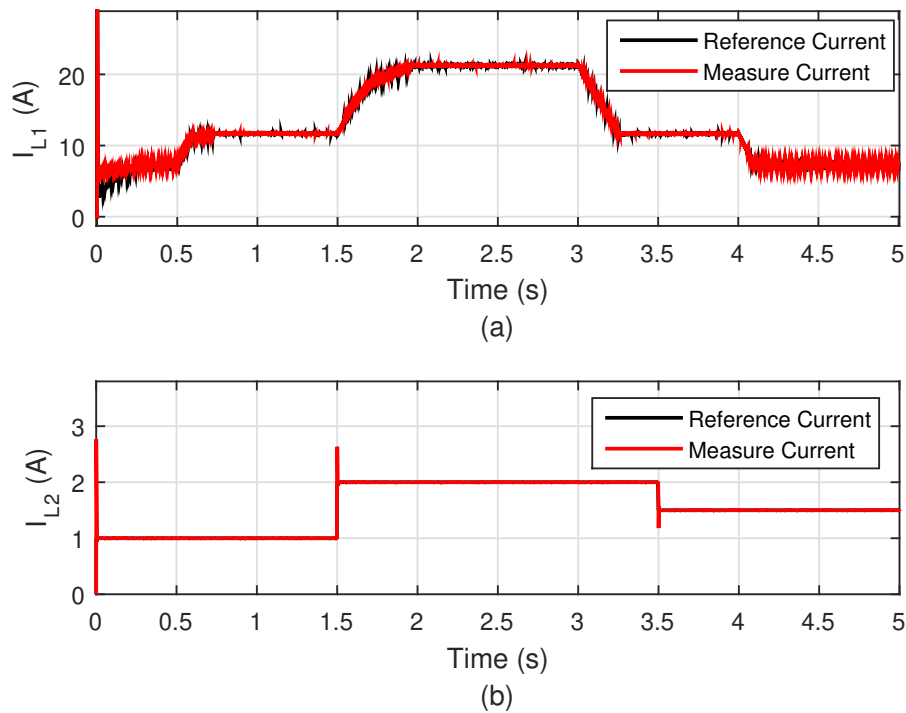

Figura 4.3: Characteristics of currents in the buck converter inductors. (a) Inductor current of the buck converter 1. (b) Current in the inductor of the buck converter 2.

It is possible to observe the lack of oscillations in the current when compared to the current I_{L2} shown in Fig. 4.3 (b). This characteristic is justified
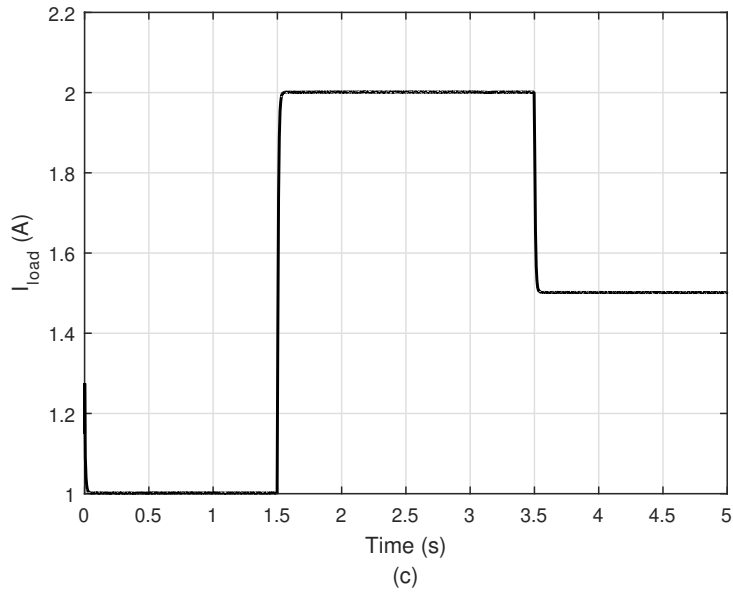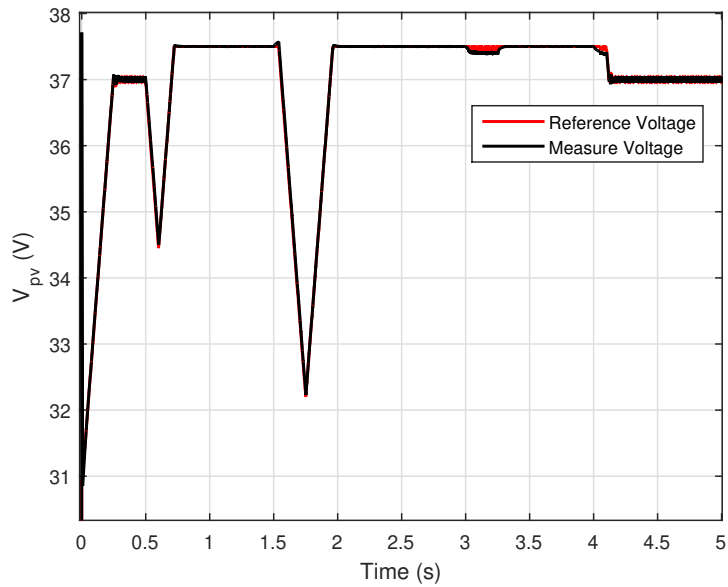
Figura 4.4: Characteristics of the Current in the EC

Figura 4.5: V_{pv} compared to the MPPT reference voltage

by the presence of the capacitor in parallel with the EC that regulates the voltage.

For the validity of the MPPT algorithm together with the controller, the reference voltage curve of the algorithm output with the bus voltage c.c. of the PVP, is shown in Fig. 4.5. It was noticed that only in the transient regime the system suffered few oscillations until in fact at the algorithm works at the ideal point and acts on small perturbations to follow the reference. Then the system operated in a good operating range and accommodation in the reference of the algorithm.

4.1.3   MPPT Efficiency Analysis

For the validity of the MPPT algorithm together with the controller, the reference voltage curve of the output of the block of the algorithm with the bus voltage c.c. of the panel, according to Fig. 4.5. It was noticed that only in the transient regime the system suffered few oscillations due to small disturbances to follow the reference; the system operated in a good range of operation and accommodation in the algorithm reference. Fig. 4.6 (a) and (b) outline the dynamic and instantaneous efficiencies for the MPPT algorithm implemented, and reveal satisfactory indexes for the operation of the photovoltaic module used, above of 90% for both.

It is observed that the instantaneous efficiency is close to 100%. For the growth or decay intervals, a decrease in efficiency was observed, but this remained at levels above 88%, validating MPPT for MPPT performance on constant irradiation levels.

On the other hand, the dynamic efficiency of a MPPT, which considers the moments of variation in the intensity of the irradiance obtained a higher index of 89%, which also reveals the positive potential of MPPT implemented, to track the maximum power. Validating the MPPT regarding the performance of the MPPT on varying levels of irradiation.

The operating point, PVP power vs. dc bus voltage, over the power panel x characteristic voltage curves of the ideal panel was observed. As shown in Fig. 4.7 it is possible to observe the dynamics of the MPPT algorithm applied, which results in the migration of the operating point on different
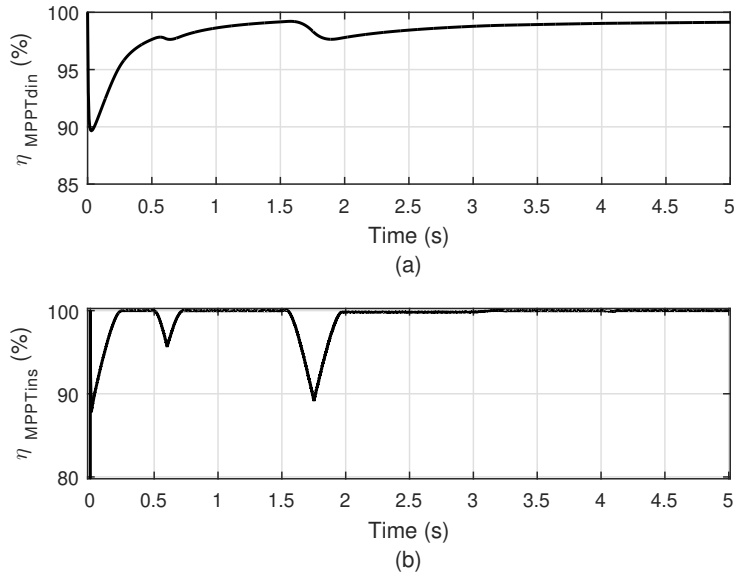
Figura 4.6: Efficiencies of the implemented MPPT algorithm, measured by the
          power developed by the photovoltaic module.
          (a) Dynamic efficiency. (b) Instantaneous Efficiency.

power curves as a function of the applied irradiance profile.

4.1.4   Power Losses Analysis

4.1.4.1   Influence of Solar Irradiation on Power Losses

Fig. 4.8. Shows how the variation of the intensity of incident solar
radiation in proportion PVP relates to losses, in particular the drive for
both IGBT and for the diodes. The diodes when compared to the IGBTs,
presented higher losses. For the switching losses of both, a negligible value of
loss was observed, due to the silicon carbide technology used in the switches.

4.1.4.2   Influence of the Reference Current on Power Losses

Loss values associated with different reference current levels were also
observed in the inductor of the buck converter 2. As shown in the Fig. 4.9.
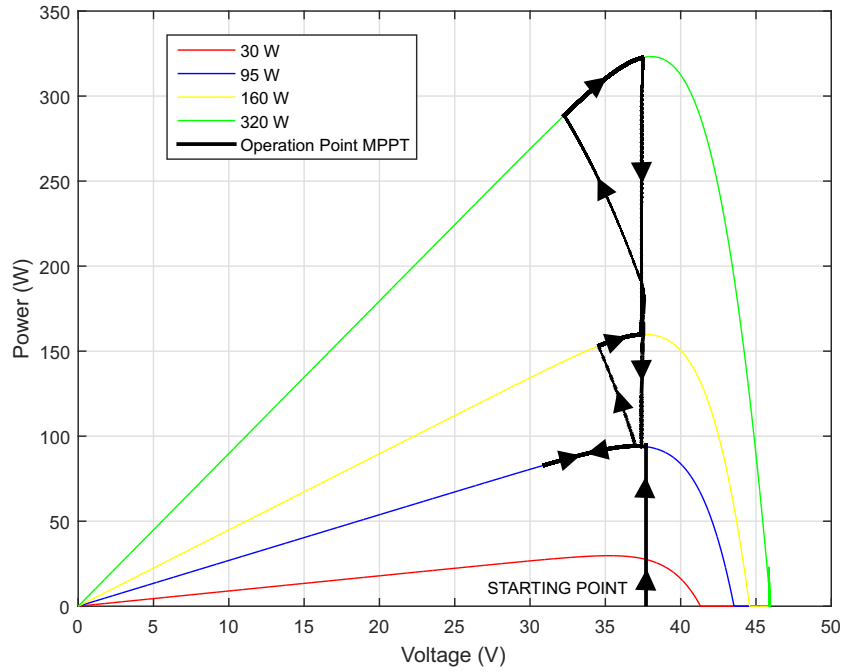
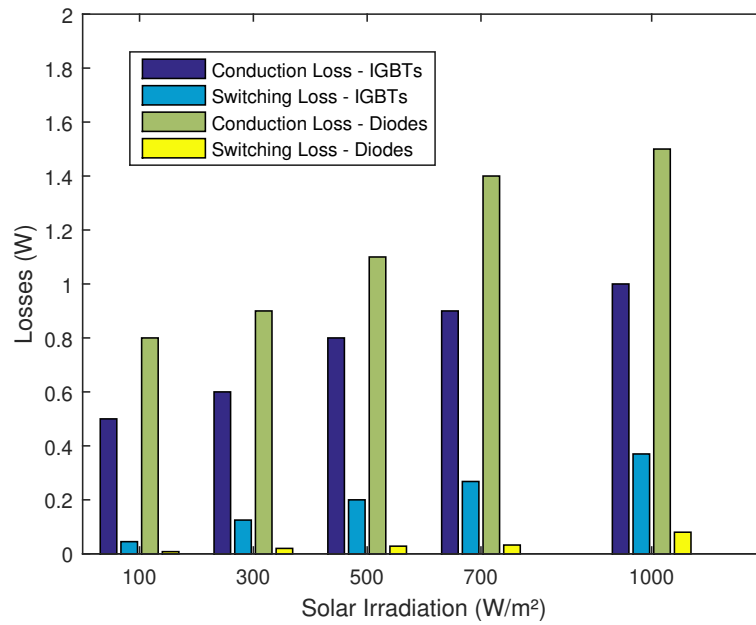Figura 4.7: Power versus Voltage curves with MPPT performance

Figura 4.8: Solar Irradiation versus Power Losses

It is possible to observe that the conduction losses of the switches used were
on the same loss range, perceptible after the values of steps of 1.5 A, which
practically stabilized in 0.8 W dissipated. Switching losses are justified as
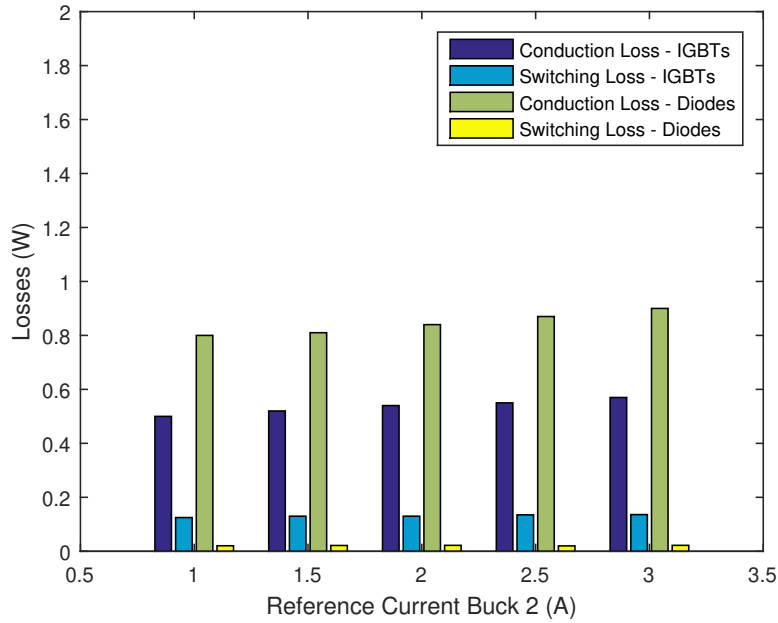argued above.

Figura 4.9: Reference Current versus Power Losses

4.1.4.3 Efficiency of AES

Finally, the efficiency of the proposed AES is analyzed. Figs. 4.10 and
4.11 shows the efficiency results for different values of solar irradiance and
reference current in the EC, respectively. The test conditions were the same
as those presented earlier in this section. The behavior similar to that obser-
ved in the switches thermal test was observed, especially in the case of solar
irradiation incident on the panel, which affects inversely proportional to ef-
ficiency. However, the index obtained from AES efficiency make the project
and its application valid.
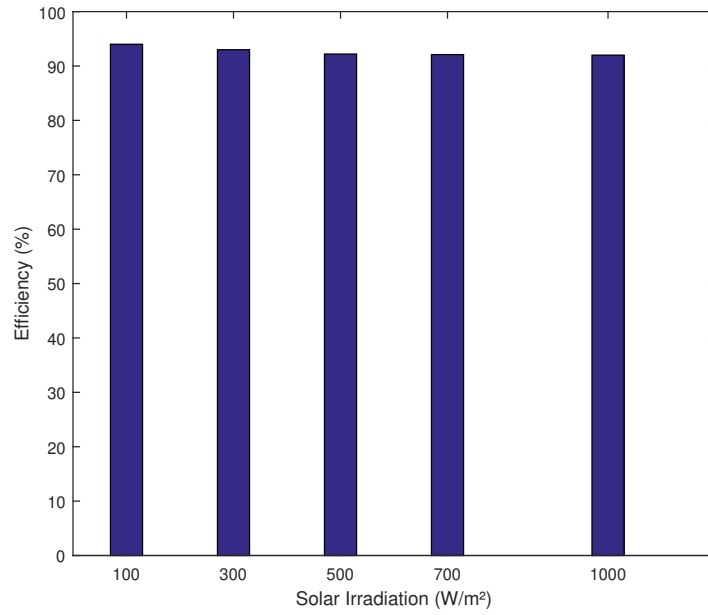
Figura 4.10: Solar Irradiation versus η_{sis}
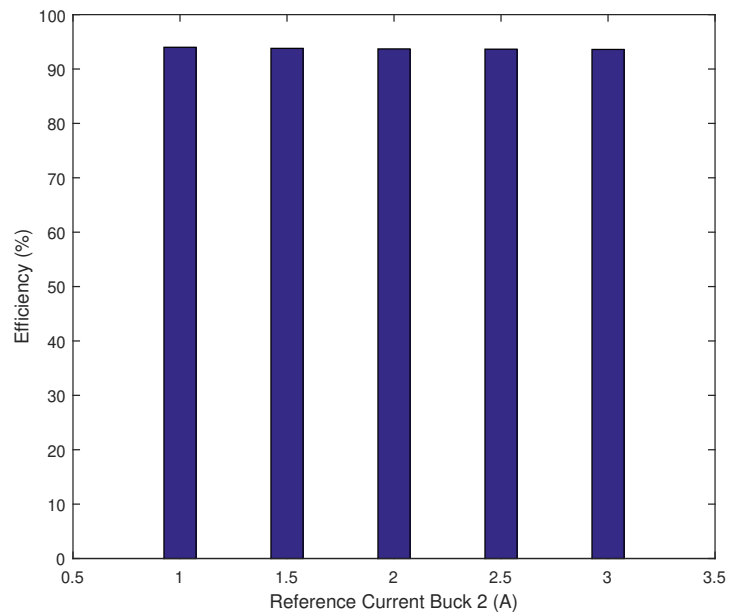
Figura 4.11: Reference Current versus η_{sis}

4.1.5   SOC Analysis Battery Discharge

In the battery discharge study, it was observed that the non-incidence of solar irradiation in the PVP causes a decrease in the battery output voltage, in a higher rhythm at the initial instants, according to Fig. 4.12 (a). In this way the voltage operates, for the instant studied, a little below the projected point of operation, without interfering in its operation.

The load state in follow a linear fall in value, as shown in Fig. 4.12 (b), showing a small variation expressed in its module. In this way, the designed battery model would be able to operate the system for much longer, affirming the autonomy of the project and later expansion in its capacity of operation.
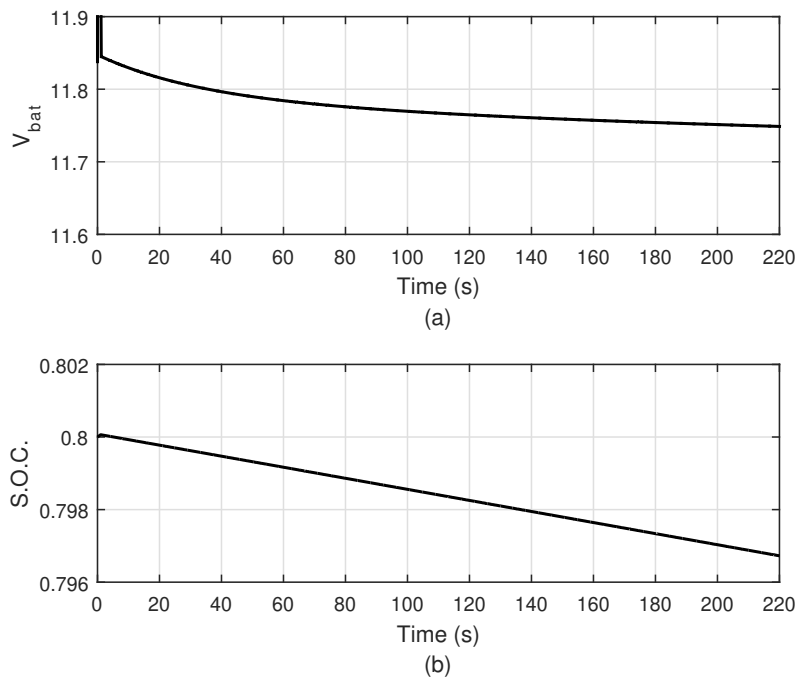

Figura 4.12: Analysis Battery Discharge. (a) SOC (b) Battery voltage

Conclusions

In this work it was proposed the integration between a photovoltaic module with a battery bank and an electrocoagulator, by means of coil converters, in order to construct a water clarification system. For this, a MPPT algorithm was implemented and the design of the voltage and current controllers was made to allow the operation of the photovoltaic module at the point of maximum energy extraction, besides providing current regulation in the EC. The method used to design the PI controllers was the allocation of poles.

The results presented resulted in an excellent integrated autonomous system. The characteristics of operations such as tensions and currents of the analyzed elements, presented in acceptable levels and expected. The levels of efficiency and power losses system revealed an excellent physical implementation capacity of the project, which would validate its application in possible structural system of water treatment. With good ability to follow the reference and good signal accommodation ranges, the control method used was validated. To control the current in the EC, in specially, a good response was obtained for the references used, evidencing the applicability of the control method.

With the results obtained, it can be concluded that the design of the use of an autonomous photovoltaic system to enable the water bleaching through an EC, and with the processes of control and extraction of maximum power, it is possible to obtain satisfactory indexes of system efficiency. As a continuity proposal, it is necessary to study the EC as a variable resistance, obtain physical dimensioning of the AES and improve the performance of the implemented MPPT algorithm, such as dP-P&O.

References

Ahmed AS, Abdullah BA, Abdelaal WGA (2016) Mppt algorithms: Performance and evaluation. International Conference on Computer Engineering Systems (ICCES) pp 461–467

Alvarez-Guerra E, Dominguez-Ramos A, Irabien A (2011) Design of the photovoltaic solar electro-oxidation (pseo) process for wastewater treatment. Chemical Engineering Research and Design 89(12):2679–2685

Barbi I (2015) Modelagem de conversores c.c.c.c. empregando modelo médio em espaços de estados. Pearson Brasil

Chen G (2004) Electrochemical technologies in wastewater treatment. Separation and purification Technology 38(1):11–41

Chen M, Rincon-Mora GA (2006) Accurate electrical battery model capable of predicting runtime and i-v performance. IEEE Transactions on Energy Conversion 21(2):504–511

Combatt MPM, Mendonça RCS, Valente GFS, Silva CM (2017) Validation of the electrocoagulation process and evaluation of the electro dissolution of electrodes in the tretment of poultry slaughterhouse wastewater. Solar Energy Materials and Solar Cells vol.40 no.4

Dubrawski KL, Mohseni M (2013) In-situ identification of iron electrocoagulation speciation and application for natural organic matter (nom) removal. Water research 47(14):5371–5380

Gao L, Liu S, Dougal RA (2002) Dynamic lithium-ion battery model for system simulation. IEEE Transactions on Components and Packaging Technologies 25(3):495–505, DOI 10.1109/TCAPT.2002.803653

Gayvoronskiy SA, Khozhaev IV, Ezangina TA (2017) Method of interval system poles allocation based on a domination principle. 2017 International Conference on Mechanical, System and Control Engineering (ICMSC) pp 245–249

Harif T, Khai M, Adin A (2012) Electrocoagulation versus chemical coagulation: coagulation/flocculation mechanisms and resulting floc characteristics. Water Research 46(10):3177–3188

Hernández-Calderón O, Félix-Navarro R, Morales-Cuevas J, Sicairos S (2011) Evaluation of the electro-coagulation process for the removal of turbidity of river water, wastewater and pond water. Revista Mexicana de Ingeniería Química 10:79–91

Holt PK, Barton GW, Mitchell CA (2005) The future for electrocoagulation as a localised water treatment technology. Chemosphere 59(3):355–367

Hussin F, Abnisa F, Issabayeva G, Aroua MK (2017) Removal of lead by solar photovoltaic electrocoagulation using novel perforated zinc electrode. Journal of Cleaner Production 147:206–216

Kourdali S, Badis A, Saiba A, Boucherit A, Boutoumi H (2014) Humic acid removal by electrocoagulation using aluminium sacrificial anode under influencing operational parameters. Desalination and Water Treatment 52(28-30):5442–5453

Ma K, He N, Liserre M, Blaabjerg F (2016) Frequency-domain thermal modeling and characterization of power semiconductor devices. IEEE Transactions on Power Electronics 31(10):7183–7193, DOI 10.1109/TPEL.2015.2509506

Marmanis D, Dermentzis K, Christoforidis A, Ouzounis K, Moumtzakis A (2015) Electrochemical treatment of actual dye house effluents using electrocoagulation process directly powered by photovoltaic energy. Desalination and Water Treatment 56(11):2988–2993

Mollah MA, Schennach R, Parga JR, Cocke DL (2001) Electrocoagulation (ec) science and applications. Journal of Hazardous Materials 84(1):29–41

Mollaha MYA, Morkovsky P, G GJA, Kesmez M, Parga J, Cockec DL (2004) Fundamentals, present and future perspectives of electrocoagulation. Journal of Hazardous Materials pp 199–210

Nguyen D, Lehman B (2008) A reconfigurable solar photovoltaic array under shadow conditions. IEEE pp 980–986, DOI 10.1109/APEC.2008.4522840

Ortiz JM, Expósito E, Gallud F, García-García V, Montiel V, Aldaz A (2007) Electrodialysis of brackish water powered by photovoltaic energy without batteries: direct connection behaviour. Desalination 208(1-3):89–100

Padhi R (2010) Pole placement control design. advanced control system design. Dept of Aerospace Engineering Indian Institute of Science, Bangalore pp Lecture of Class, 21

Pihl E, Kushnir D, Sandén B, Johnsson F (2012) Material constraints for concentrating solar thermal power. Energy 44(1):944–954

Pinto VG, Heller L, Bastos RKX (2012) Drinking water standards in south american countries: convergences and divergences. Journal of water and health 10(2):295–310

Pirkarami A, Olya ME, Tabibian S (2013) Treatment of colored and real industrial effluents through electrocoagulation using solar energy. Journal of Environmental Science and Health, Part A 48(10):1243–1252

Prieb, Massen CW (2011) Determinação da eficiência de seguimento de máxima potência de inversores para sistemas fotovoltaicos conectados à rede de distribuição. Universidade Federal do Rio Grande do Sul Escola de Engenharia Programa de Pós-Graduação em Engenharia Mecânica

Rashid MH (July 29, 2013) Power electronics: Circuits, devices & applications. Pearson 4th Edition

Rinaldi N (2001) On the modeling of the transient thermal behavior of semiconductor devices. IEEE Transactions on Electron Devices 48(12):2796–2802, DOI 10.1109/16.974706

Schonberge J (2010) Modeling a lithiumion cell using plecs. Plexim GmbH 1(1):1–5

Sera D, Kerekes T, Teodorescu R, Blaabjerg F (2006) Improved mppt method for rapidly changing environmental conditions. IEEE ISIE pp 1420–1435

Sera D, Teodorescu R, Rodriguez P (2007) Pv panel model based on datasheet values. 2007 IEEE International Symposium on Industrial Electronics pp 2392–2396, DOI 10.1109/ISIE.2007.4374981

Sera D, Mathe L, Kerekes T, Spataru SV, Teodorescu R (2013) On the perturb and observe (p&o) and incremental conductance mppt methods for pv systems. IEEE Journal of Photovoltaics pp 1070–1078

Smith CS, Corripio AB (2008) Principles and practice of automatic process control. John Wiley and Sons 3

Stroe DI (2014) Lifetime models for lithium ion batteries used in virtual power plants. Dissertation submitted to degree of Doctor of Philosophy in Electrical Engineering

Ulu F, Barışçı S, Kobya M, Särkkä H, Sillanpää M (2014) Removal of humic substances by electrocoagulation (ec) process and characterization of floc size growth mechanism under optimum conditions. Separation and Purification Technology 133:246–253

Valero D, Ortiz JM, Exposito E, Montiel V, Aldaz A (2008) Electrocoagulation of a synthetic textile effluent powered by photovoltaic energy without batteries: direct connection behaviour. Solar Energy Materials and Solar Cells 92(3):291–297

Villalva MG (2010) Conversor eletrônico de potência trifásico para sistema fotovoltaico conectado à rede elétrica. UNICAMP - Universidade Estadual de Campinas, FEEC 1(1):1–292

Villalva MG, Gazoli JR, Filho ER (2009) Comprehensive approach to modeling and simulation of photovoltaic arrays. IEEE Transactions on Power Electronics 24(5):1198–1208, DOI 10.1109/TPEL.2009.2013862

Yıldız Y, Koparal A, Keskinler B (2008) Effect of initial ph and supporting electrolyte on the treatment of water containing high concentration of humic substances by electrocoagulation. Chemical Engineering Journal 138(1):63–72

Yildiz YS, Koparal AS, Irdemez S, Keskinler B (2007) Electrocoagulation of synthetically prepared waters containing high concentration of nom using iron cast electrodes. Journal of hazardous materials 139(2):373–380

Zhang S, Zhang J, Wang W, Li F, Cheng X (2013) Removal of phosphate from landscape water using an electrocoagulation process powered directly by photovoltaic solar modules. Solar Energy Materials and Solar Cells 117:73–80